Bulletin of Volcanology (2024) 86:24
https://doi.org/10.1007/s00445-024-01727-7

RESEARCH ARTICLE

# Large debris avalanche and associated eruptive event at Samalas volcano, Lombok, Indonesia

**Mukhamad Ngainul Malawani[1] · Franck Lavigne[2] · Karim Kelfoun[3] · Pierre Lahitte[4] · Danang Sri Hadmoko[1] · Christopher Gomez[5] · Patrick Wassmer[6] · Syamsuddin Syamsuddin[7] · Audrey Faral[2]**

Received: 1 August 2023 / Accepted: 25 February 2024 / Published online: 2 March 2024


## Abstract

We propose a vast area in the middle of Lombok, Indonesia, dominated by hummock hills, is a debris avalanche deposit (DAD). We define this > 500 km$^2$ area as Kalibabak DAD that may originate from Samalas volcano. No descriptions of the morphology, stratigraphy, mechanism, and age of this DAD have yet been reported; this contribution bridges this research gap. Here we present morphological and internal architecture analysis, radiocarbon dating, paleotopographic modeling, and numerical simulation of the DAD. We also present geospatial data e.g., topographical and geological maps, digital elevation models (DEMs), satellite imagery – in combination with stratigraphic data constructed from field surveys, archived data, and electrical resistivity data. Results show that the DAD was formed by a sector-collapse of Samalas volcano and covers an area of 535 km$^2$, with a deposit width of 41 km and a runout distance up to 39 km from the source. The average deposit thickness is 28 m, reaching a measured local maximum of 58 m and a calculated volume of ~ 15 km$^3$. Andesitic breccia boulders and a sandy matrix dominate the deposit. Using ShapeVolc, we reconstructed the pre-DAD paleotopography and then used the reconstructed DEM to model the debris avalanche using VolcFlow. The model provides an estimate of the flow characteristics, but the extent of the modelled deposit does not match the present-day deposit, for at least two reasons: (i) the lack of information on the previous edifice topography that collapsed, and (ii) limited understanding of how DADs translate across the landscape. Fourteen radiocarbon dating samples indicate that the DAD was emplaced between 7,000–2,600 BCE. The DAD's enormous volume, vast extent and poorly weathered facies strongly suggest that it was not triggered by a Bandai-type debris avalanche (solely phreatic eruption), but more likely by a Bezymianny-type (magmatic eruption). This event was potentially triggered by a sub-Plinian or Plinian eruption (high eruption column with umbrella-like cloud) dated ~ 3,500 BCE, which produced the Propok pumice fall deposits.

**Keywords** Debris avalanche · Paleotopography · Landscape evolution · Samalas volcano

## Introduction

Volcanic sector collapse and associated debris avalanches transform whole volcanic structures, generating typical hummocky structures (Siebert 1984; Hunt et al. 2018).

Editorial responsibility: Editorial responsibility: V. Acocella

✉ Mukhamad Ngainul Malawani
malawani@ugm.ac.id

[1] Faculty of Geography, Universitas Gadjah Mada, Yogyakarta, Indonesia

[2] Université Paris 1 Panthéon-Sorbonne, Laboratoire de Géographie PhysiqueUMR 8591, UP1, CNRS, UPEC, Thiais, France

[3] Laboratoire Magmas Et Volcans, Université Clermont Auvergne, Clermont-Ferrand, France

[4] Géosciences Paris Sud (GEOPS), Université Paris-Saclay, Orsay, France

[5] Faculty of Maritime Sciences, Kobe University, Kobe, Japan

[6] Faculty of Geography and Territory Planning, University of Strasbourg, Strasbourg, France

[7] Faculty of Mathematics and Natural Science, Mataram University, Lombok, Indonesia

Examples of significant volcanic sector collapses due to a lateral eruption include the eruption of Bezymianny (Russia) in 1956 (Siebert et al. 1987; Belousov et al. 2007), Mount St. Helens (USA) in 1980 (Voight et al. 1985; Glicken 1996), and Soufrière Hills (Montserrat) in 1997 (Belousov et al. 2007). Furthermore, debris avalanches can create cascading hazards, particularly when entering a lake or the sea (Camus et al. 1992; Capra et al. 2002), such as the tsunami generated on 22 December 2018 following the Krakatoa sector collapse (Grilli et al. 2019). The global inventory of debris avalanches has registered 1001 events from 594 volcanoes in 52 countries (Dufresne et al. 2021). Indonesia has over 130 volcanoes and 70 cases of debris avalanches have been inventoried (MacLeod 1989; Dufresne et al. 2021), but only a few studies have attempted to provide the detailed characteristics of their deposits. Some historical debris avalanche events left massive deposits covering wide areas emanating from the volcano, such as Gede (MacLeod 1989), Galunggung (Bronto 1989), Raung (Siebert 2002; Moktikanana et al. 2021), Merapi (Bronto et al. 2014), and Papandayan in 1772 CE (Pratomo 2006; Siebert & Roverato 2021). This last event is believed to have caused 2,957 fatalities (Dufresne et al. 2021).

Dome intrusions and phreatic explosions are examples of the main triggers of debris avalanches as they can cause structural instability that may lead to the collapse of volcanic structures. More rarely debris avalanches can also be triggered by earthquakes, heavy rain, or snowmelt (Siebert 1984; Voight et al. 1983). The velocity of a debris avalanche can reach ~ 50 to-150 m/s, and the distance covered tens of kilometers from the source (Ui et al. 1986; Lomoschitz et al. 2008; van Wyk de Vries and Davies 2015). Debris avalanches can significantly modify the volcanic landscape and surroundings (Cortés et al. 2010). On the volcano, the sector collapse generally leaves a horseshoe-shaped scar, which can lead to the total collapse of the volcano or be of smaller amplitude and can even disappear with the growth of a new cone (Bronto et al. 2014). In the surrounding areas, the transported material usually creates a hummocky terrain in the medial to distal area (Siebert 1984; Lomoschitz et al. 2008; Vezzoli et al. 2017). Hummocks have a distinctive hilly morphology that is easily differentiated from the surrounding land, thus becoming the signature of a debris avalanche deposit (DAD) (Ui 1989); Paguican et al. 2014; Hayakawa et al. 2018).

The spatial distribution of DADs and the formation of hummocks are influenced by the material composition (Bernard et al. 2009; Salinas & López-Blanco 2010). The deposit is formed of mainly breccia and unconsolidated materials of various sizes, such as sand, gravel, pebbles, and large boulders (Roverato et al. 2011). Depending on its lithofacies, a DAD can be divided into three types: syn-eruptive, hybrid (gravitational flows, coarsely stratified, poorly sorted); and lahar-transform (rapid flows and hyperconcentrated flows) (Bernard et al. 2019). The classical parameter H/L can be used to illustrate debris avalanche mobility, where H value represents the maximum elevation source or drop height of the displaced mass, and L is the run-out distance (Ui et al. 1986; Siebert et al. 1995). The H/L ratio will generally decrease when the volume of deposits is large (Ui et al. 1986). The shape of the hummocks can also be used to infer the direction of the flow, especially the elongated hummocks that are parallel to the direction of flow (Dufresne & Davies 2009). A group of aligned hummocks that coincide with the flow direction is called a hummock train (Shea et al. 2008).

The center of Lombok Island (Indonesia) is covered by a widespread hilly landscape (> 500 $km^2$). Despite its extent, very limited research on it has been carried out and preliminary investigation has not provided a detailed analysis of the morphology, lithology, age, nor depositional process (Malawani et al. 2020). It has been shown that the hummocky hill on the center of Lombok played an essential role in the distribution of the 1257 CE pyroclastic density current (PDC), as well as the geomorphologic evolution of the island (Vidal et al. 2015; Mutaqin et al. 2019). Although previous work has tentatively interpreted this hilly area as a DAD, a typical horseshoe-shaped scar is missing and warrants additional study. This present study aims to: a) confirm that a vast area of hummocky hill is a DAD emanating from Samalas volcano, b) analyze the internal structure and stratigraphy of the deposit, and c) reconstruct pre-event topography and flowing mechanism, as well as to date this event.

## Geological Setting

The Samalas volcano is part of the Rinjani Volcanic Complex, located on Lombok Island (Fig. 1). Samalas volcano erupted in 1257 CE, leaving a ~ 6 km wide caldera (Lavigne et al. 2013; Vidal et al. 2015). This caldera is filled by the Segara Anak lake and a rising volcano called the Barujari, which was formed from lava ejected from a new vent in the eastern part of the lake (Rachmat et al. 2016). Six main lava flows were recorded following several effusive eruptions of Barujari in 1944, 1966, 1994, 2004, 2009, and 2015 (Solikhin et al. 2010; Abdul-Jabbar et al. 2019). The geological map of Indonesia (1:100,000) displays a large volcaniclastic deposit called Kalibabak Formation (TQb), which is characterized by volcanic breccia rocks (Mangga et al. 1994) (Fig. 1) in the southern part of this volcanic complex. The deposit is poorly sorted, with a random fabric, and contains angular-shaped rock fragments (Maryanto 2009). This formation is predominantly composed of andesitic materials, such as porphyry andesite, basaltic andesite, and basalt (Maryanto et al. 2009). However, the Kalibabak Formation (TQb) is present in two parts in the west and in the

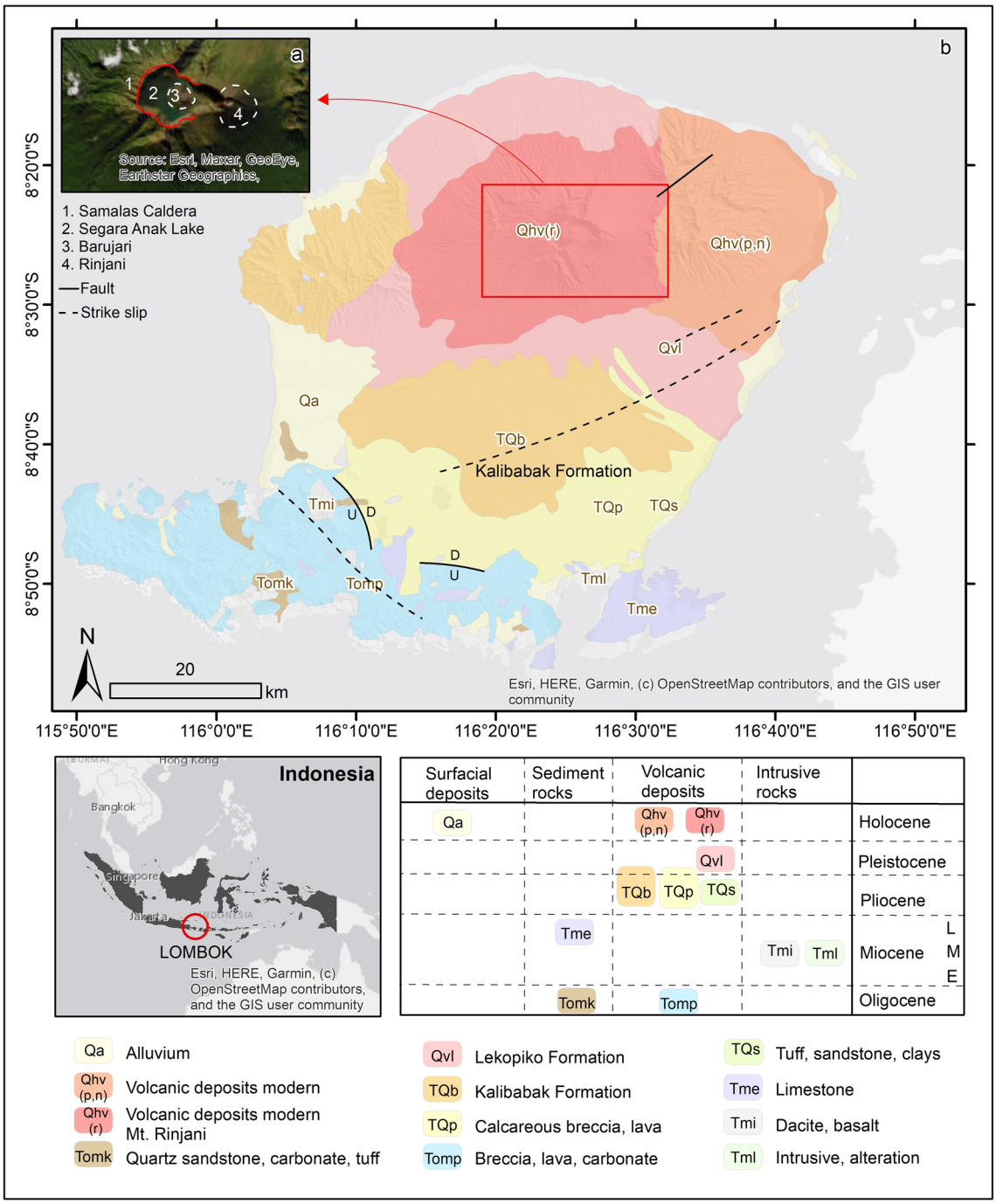


**Fig. 1** Geological Map of Lombok. This map shows that Lombok is composed of volcanic complexes in the north, sedimentary materials in the middle, and uplifted tertiary mountain ranges in the south

central part of the island. Despite having the same geologic name, these two formations have a distinct morphology and likely different origins. This formation in the western part forms a strongly eroded mountainous complex, whereas in the central part it covers a larger area, with numerous small hills. The subsequent description will focus on TQb in the central part of Lombok Island.

The outcrops along the riverbanks and on the road-side show that the Kalibabak Formation is composed of heterogenic lithic fragments, dominated by pebbles (5–50 cm) and boulders (up to 2.5 m). Data gathered from previous studies of the Kalibabak Formation (Maryanto 2009) show that the grain size of breccia matrices of this formation is poorly sorted with a matrix of sandy gravel (71%). The clay

content is very low (< 5%), suggesting that the water content was limited during deposition (Maryanto 2009). Resistivity investigations of the Kalibabak Formation revealed that it is up to 21 m thick, with no significant water content (Sukandi 2017).

The shape of the Kalibabak Formation is wider in the middle and lobate at the distal area (Fig. 1). To the north of the Kalibabak, the younger Lekopiko Formation (Fig. 1) is made of a mixture of pyroclastic materials from lahars and pumiceous tuffs (Mangga et al. 1994). The Lekopiko Formation was formed by the syn- and post-eruptive materials of the 1257 CE eruption of Samalas and its limit on the geological map corresponds to the limit of the Samalas deposit map provided by Lavigne et al. (2013) and Vidal et al. (2015). Both formations have been attributed to the Samalas volcano. The characteristics of Kalibabak Formation, both the surface and subsurface structure strongly suggest that this formation is a DAD of a single event and has no connection with the TQb in the west. Since it is identified as Kalibabak Formation on the geological map, we called this massive deposit originating from Samalas volcano the Kalibabak DAD.

## Methodology

### Morphological Analysis

The morphological analysis of the whole DAD and individual hummocks was performed. First, we acquired a set of satellite imagery and the digital elevation model (DEM). Two imageries from Sentinel-2 (https://apps.sentinel-hub.com/eo-browser/) and World Imagery from ESRI in ArcMap have been used. The DEMs data used in this research is the DEMNAS (DEM *Nasional*) from the Geospatial Information Agency of Indonesia (https://tanahair.indonesia.go.id/demnas/#/) and SRTM (*Shuttle Radar Topography Mission*) derived from https://earthexplorer.usgs.gov. DEMNAS has been developed from several data sources: IFSAR (5 m resolution), TERRASAR-X (5 m resampling resolution), and ALOS PALSAR (11.25 m resolution) using the EGM2008 vertical datum. The spatial resolution of DEMNAS is 0.27 arc-seconds (~8 m). Completing this dataset, the (12.5 m line-intervals) topographic map of Indonesia (*Rupa Bumi Indonesia*) has also been used.

The hummocks were mapped to calculate their spatial distribution and classify them according to morphological parameters. These parameters are the hummock shape in 2D and 3D (Bernard et al. 2021), the distance of each hummock from the present caldera (Siebert 1984; Hayakawa et al. 2018), and the area/size ratio of each hummock (Yoshida 2014). A plot of the relationship between the hummock size and distance from the source was also constructed to analyse the spatial distribution of morphology, as hummock size has shown to decrease with distance from the source (Yoshida 2013).

After completing the identification of individual hummocks, the next step was to delineate the DAD boundary (Fig. 2) using the outermost hummocks and considering the outer limit of the Kalibabak Formation as the maximum extent of the DAD. Site surveys encircling the edges of the Kalibabak Formation suggested that the geologic boundary of this formation differs from the actual boundary across the field, particularly in the east. The revised boundary, which is then defined as the DAD boundary, is extended to the coastline in the east. The morphological characteristics also relied on the profile line, slope, aspect, and drainage accumulation, as they are commonly used to characterize the morphology of landforms (Garajeh et al. 2022). In the DAD area, spatial differentiation based on of hummock density was calculated within the DAD boundaries, to identify the clustering of hummocks (hummock train) that are parallel to the flow direction (Procter et al. 2021; Shea et al. 2008). The deposit domains (toreva, hummock, and piedmont domains) were also mapped based on the morphological characteristics (Andrade and van Wyk de Vries 2010; Paguican et al. 2014; Norini et al. 2020).

### Subsurface Analysis

#### A. Stratigraphic Survey

Stratigraphic data from 26 sites were collected from field surveys in exposed areas of open-cuts sections (from mining activity and road construction) and riverbanks (Fig. 2). Visual observation on the outcrop is helpful in identifying DAD facies (Valverde et al. 2021). To complement the outcrops, data from 10 sediment cores supplied by the Energy and Mineral Resources Agency (ESDM) of West Nusa Tenggara Province were collected (Maryanto 2009; Maryanto et al. 2009). Stratigraphic data were used to measure the thickness of the DAD, which is crucial for calculating the volume and reconstructing the topography of the former Samalas's edifice.

#### B. Resistivity Measurement

A resistivity measurement campaign was carried out in conjunction with LIPI (now BRIN, *National Research and Innovation Agency*) and UNRAM (University of Mataram). Measurements using a Dipole-Dipole configuration were conducted with a span of ~1000 m in total at Surabaya-Lepak, East Lombok (Fig. 2). The locations were chosen to study subsurface conditions in the distal part of the DAD which is not covered by core or outcrop data and to verify the DAD boundary. Measurements were carried out using

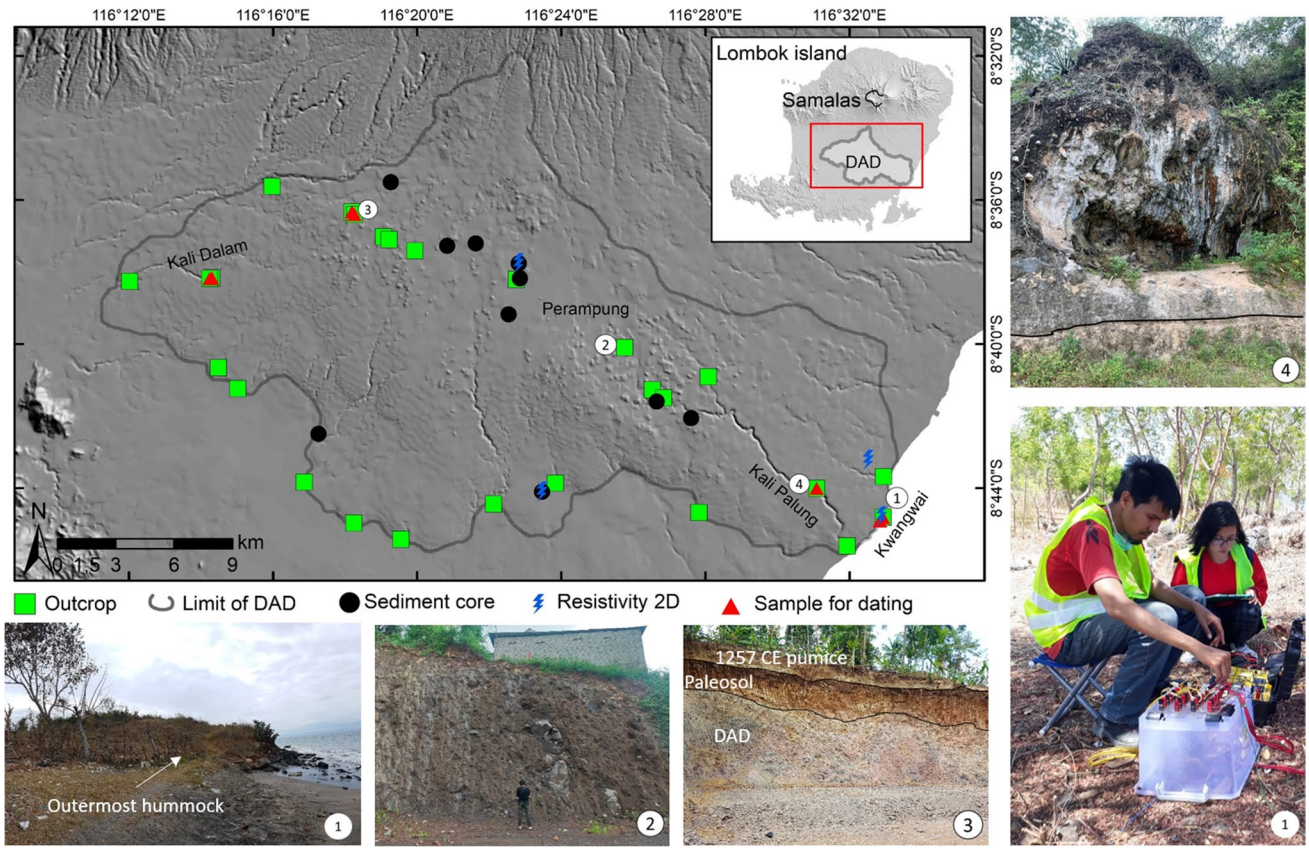


**Fig. 2** Map of sampling sites: outcrop, core, resistivity, and dating. Photos of field survey: the outermost hummock (1), opencut hummocks (2 and 3), escarpment in the river valley (4), and resistivity measurement (5)

the SuperSting R8/IP with 56 swift electrodes. This configuration used 10 m spacing between electrodes, allowing us to observe the subsurface condition down to ~142 m deep. The data were then inverted into a 2D resistivity profile.

Resistivity measurements using a Wenner configuration were also carried out on eight lines (150-300 m), including three at Jenggik (the upper DAD zone), three at Kwang Wai (in the hummocky hills), and two at Janapria (the distal zone) (Supplementary Material: Table S1). All resistivity results were interpreted to delineate the DAD layer boundary on the basis of a resistivity value corresponding to the stratigraphic layers of two cores referenced at Jenggik and Janapria and in comparison with previous measurements within the Kalibabak Formation boundary (Wiranata et al. 2018). The resistivity measurement helps to characterize the depositional pattern and reconstruct the paleosurface (Malawani et al. 2023).

## Paleo-topographic modeling

To reconstruct the morphology of Samalas volcano before the debris avalanche, the pre-collapse topography was modeled using the ShapeVolc model (Lahitte et al. 2012; Dibacto et al. 2020). For this reconstruction, we first identified and separated the volcanic sectors of Samalas volcano that were part of the "Old Samalas" (< 1257 CE) from those of the Young Samalas (Fig. 3a). From this division, the ridges of the Old Samalas were used as constraining points (CPs) to model the pre-collapse edifice (Fig. 3b: red point), as they are relatively stable compared to the other features more prone to erosion and deposition (Dibacto et al. 2020). Lowland CPs (tallow point) were generated by subtracting the deposit thickness (field data) from the current DAD topography, based on stratigraphic analysis (Fig. 3b).

## Metrics calculation

DAD metrics (Table 1 and Fig. 4) were calculated from the 11 parameters summarized by Bernard et al. (2021), using a combination of the topographic data and pre-DAD topography (Fig. 4). Although most parameters can be calculated directly from the topographic map, the calculated DAD volume may be subject to considerable error (Bernard et al. 2021). To overcome this issue, we applied two methods to calculate the volume: firstly, by using the calculation formula shown in Table 1, and secondly, using a

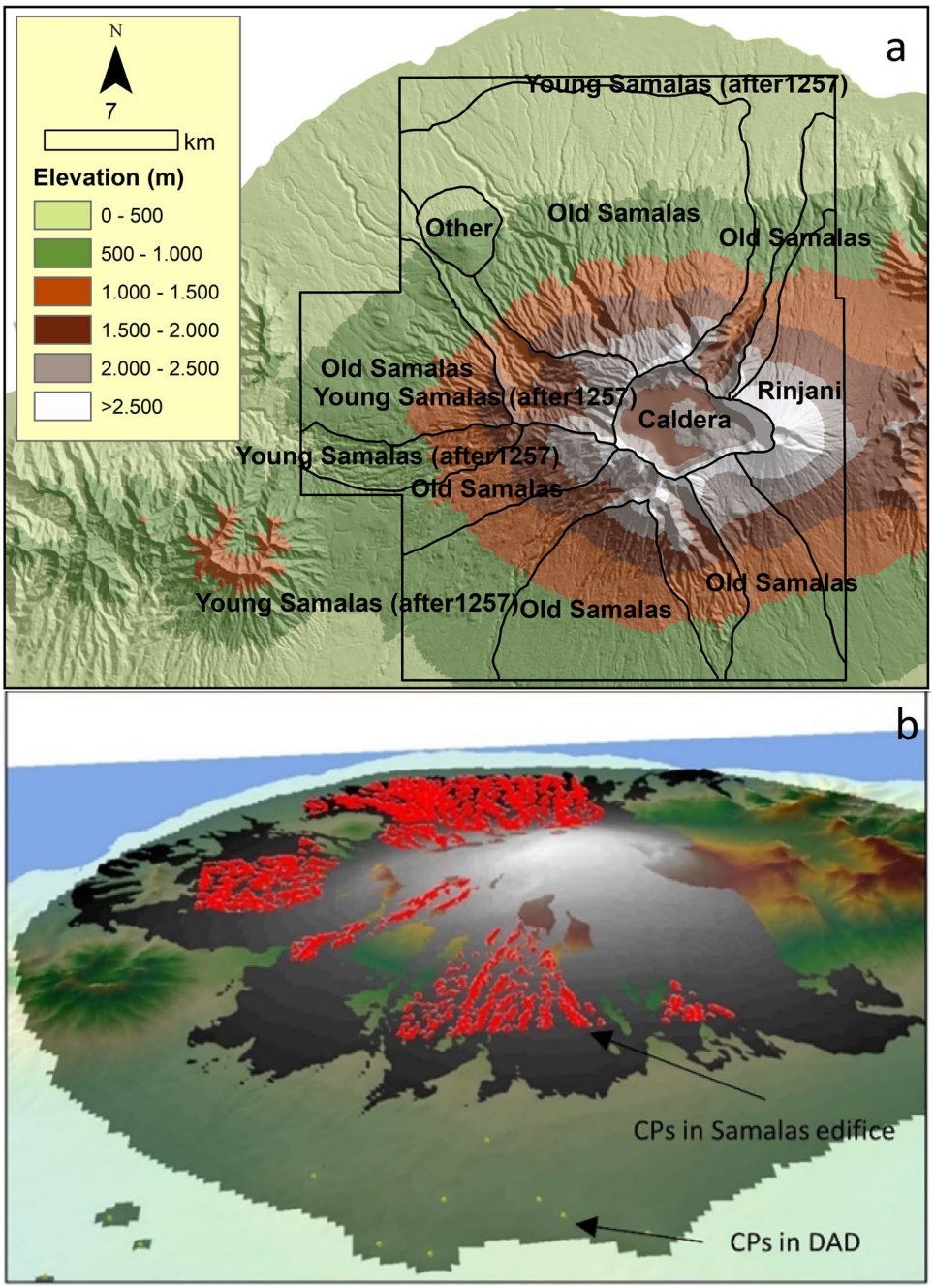


**Fig. 3** Topography differentiation of the Samalas edifice between Old and Young Samalas (**a**) to generate constraining points (CPs) for reconstructing the pre-collapse topography (**b**). Red points are CPs in the Samalas edifice, yellow are CPs in the DAD, and grey-shaded section is the reconstructed Samalas's pre-collapse topography

DEM subtraction method employing the current DEM and the pre-avalanche DEM (PDEM) (Malawani et al. 2023). The PDEM represents the topography before the DAD, which was created by kriging interpolation of the pre-DAD points (CPs in Fig. 3). The volume difference between the current DEM and the PDEM within the area of DAD defines the volume of Kalibabak DAD. A similar method to calculate volume using the subtraction method was applied to the debris avalanche deposit of the Milo Lahar sequence and the opening of the Valle del Bove on the Etna volcano (Italy) (Calvari et al. 2004). In the case of the Kalibabak DAD, although the pre-avalanche topography is a result of reconstruction and data of DAD thickness is also limited, the average volume from these two measurements is the best estimation we can obtain. However, due to the limited number of cores used to calculate the DAD thickness, an uncertainty value needs to be considered. Since cores were extracted at every 1 meter depth, we set this value as the uncertainty of the DAD thickness. The volume uncertainty calculation is then defined by multiplying the uncertainty of depth (±1 m) with the DAD area.

**Table 1** Description and calculation formula of debris avalanche metrics (Bernard et al. 2021)

| No | Parameter / Acronym | Description |
|---|---|---|
| 1 | Deposit length / $L_D$ | Distance from the front to the tail |
| 2 | Deposit width / $W_D$ | Maximum distance between the margins |
| 3 | Deposit area / $A_D$ | Surface area in plain view |
| 4 | Deposit height / $H_D$ | Altitude difference between the tail and the front |
| 5 | Deposit declivity / $<_D$ | Average slope ($<_D = H_D / L_D$) |
| 6 | Deposit thickness / $T_D$ | Average thickness |
| 7 | Deposit volume / $V_D$ | Volume calculation ($V_D = A_D / T_D$) |
| 8 | Deposit aspect ratio / $AR_D$ | Ratio between the average thickness and the radius of circle area ($AR_D = T_D / A_D/\square$) |
| 9 | Runout distance / L | Distance from the head (scar) to the front |
| 10 | Drop height / H | Altitude difference between the maximum pre-landslide topography and the front |
| 11 | Friction coefficient / H/L | Ratio between the drop height and runout distance |

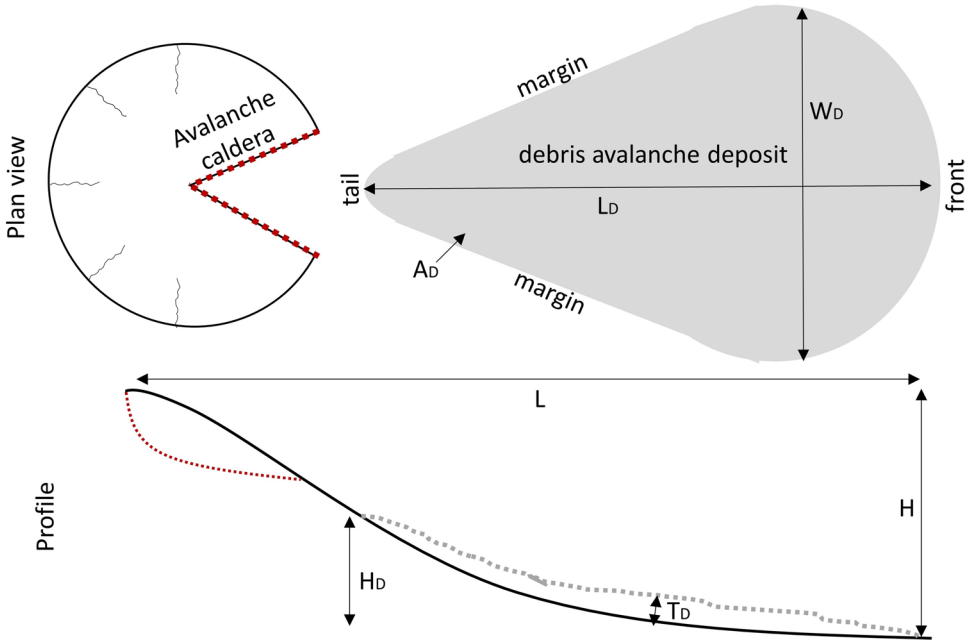


**Fig. 4** Sketch and cross-section of debris avalanche metrics

## Debris Avalanche Modeling

To explore the shape, location and orientation of the avalanche caldera, we used VolcFlow numerical modeling (Kelfoun & Druitt 2005; Kelfoun 2011) to reproduce the observed DAD. VolcFlow has been designed to simulate volcanic flows including debris avalanches on land or underwater (Kelfoun & Druitt 2005; Kelfoun et al. 2010; Paris et al. 2017). VolcFlow needs the pre-collapse topography, the topography of the sliding surface, as well as the rheological parameters of the avalanche. VolcFlow simulations used the paleotopography reconstructed using ShapeVolc, where the Samalas summit was fully restored and the DAD deposit in the lower part was removed. Several shapes and orientations of the sliding surface were explored using a spoon-like morphology defined by:

$$z_s = e^{-a \times r} + b\theta^2 + z_{\min} \quad (1)$$

In the Eq. 1, $r$ is the radial distance and $\theta$ the tangential distance. The parameters $a$, $b$ and $z_{\min}$ define the depth and the width of the avalanche caldera and its elevation. We varied them while imposing a destabilised volume compatible with the field observations (~15 $km^3$). We also varied the orientation of the radial distance from N180 to N210. Based on previous studies (e.g., Kelfoun & Druitt 2005; Kelfoun et al. 2010; Paris et al. 2017), we have used a rheology made by a yield strength $T$ and a turbulent stress $\xi\rho u^2$ where $\rho$ is the avalanche density and $u$ its velocity (Kelfoun 2011). For

debris avalanche previously studied, the value of $T$ is about 50 kPa and the value of $\xi$ (Voellmy coefficient) lower than 0.01.

### Radiocarbon Dating

Paleosols and detritus sediments above and below the DAD were sampled for dating the debris avalanche event (Fig. 2). We collected samples of paleosols below the DAD to estimate the maximum age of the event, and above the DAD to estimate the minimum age. This bracketing method is based on the method applied at the Antuco volcano (Chile) (Romero et al. 2022), because dating of past debris avalanches is particularly challenging when no charcoals are found (Grosse et al. 2022), as it was the case in this research.

Dating was performed on ten samples from four different sites, consisting of four paleosols above the DAD, as well as four paleosols and two detritus sediments below the DAD. The paleosols above the DAD layer are buried by the syn-eruptive deposits of the 1257 CE Samalas eruption and have formed relatively thick soil (~1 m). Two paleosols below DAD at a distance of ~300 m one from another were collected from Kali Dalam river valley (Fig. 2). Paleosol samples from Kwang Wai beach were collected on the marine notches (hummock cliff). The outermost hummock in Kwang Wai beach was chosen as the sampling site because this location is predicted to have minimum paleosol erosion. Two detritus sediments were collected from Kali Palung river valley and exposed beach-floor at Kwang Wai beach (Fig. 2). The results of laboratory analysis are given as age BP (Before Present-before 1950 CE). These ages were then calibrated using Calib 8.2 (http://calib.org/calib/) (Stuiver and Reimer 1993) employing the mixed curve of IntCal20 and SHCal20 because Indonesia is located in the area between two seasonal Inter-Tropical Convergence Zone (ITCZ) (Hogg et al. 2020) (Supplementary Material: Table S4). The calibrated ages were then correlated to the previous dating of Rinjani Volcanic Complex eruption chronology since the Holocene (Nasution et al. 2004; Métrich et al. 2017).

## Results

### Morphological Characteristics

To describe the morphological characteristics of DAD in Lombok, we initially present the morphological data of individual hummocks. The two-dimensional (2D) shape of hummocks is defined by the circular form of individual hummock boundaries: elongated, rectangular, polygonal, and rounded hummocks. A total of 1704 hummocks have been identified. Rounded hummocks dominate the study area, with 771 (Fig. 5a). Elongated hummocks that indicate the mass flow direction comprise 16% of the total (265 hummocks). The three-dimensional (3D) form of hummocks in conical and ridge has an almost similar distribution, comprising 41% and 43% of the total, whereas the pyramidal hummock is only 3% (44 hummocks) (Fig. 5b). The mapping results show that the hummock shape is not related to the sliding distance. All hummock shapes are well distributed across the DAD body. However, rounded hummocks have the farthest coverage compared to the other shapes. Similarly, all hummock forms are well distributed in the DAD body, except for the pyramidal form, which is only present in the middle area.

The farthest hummock is 39.5 km from the present caldera, whereas the nearest is 18.6 km. The majority of hummocks are distributed around 30-31 km from the present caldera rim (Fig. 6a). The outermost hummock was identified in the Kwang Wai beach, which formed a ~3 m high cliff. In this location nearly half of the hummock hill has been eroded by the sea waves. At distances below 23 km, the number of hummocks is relatively low, whereas further than 23 km from the caldera rim, the distribution gradually increases to a maximum distribution at 31 km. After reaching this distance, the hummocks' density rapidly decreases (Fig. 5c, d). Large hummocks with an area >8 ha are distributed across a distance of 22-23 km, whereas the average size of hummocks (2 ha) is distributed along the entire DAD body (Fig. 6b). According to their distribution, hummocks of the Kalibabak DAD do not follow the general pattern of hummock distribution, i.e., hummocks size decreases with increasing distance from the source. The hummocks with above-average size were found at a maximum distance of 30 km. The linear correlation also suggests that the relationship between area and distance is very low, with R-squared value of 0.02.

The next characterization is the surface morphology of the area within the DAD boundary. The entire DAD is dominated by relatively flat slopes, indicating the intra-hummock zone. Steep slopes are scattered throughout the river valleys, such as Kali Dalam to the west and Kali Palung to the east (Fig. 7a). Slope information indicates that river valleys have the steepest slope, due to the intense erosion in this area. The post-collapse deposition process can be detected by analyzing the flow accumulation. This parameter shows that the drainage system is centered on three river valleys, namely Kali Dalam to the west, Kali Dodokan to the middle, and Kali Palung to the east (Fig. 7b). Three dominant aspects (azimuth of terrain surface) are also present in the study area: southeast, south, and southwest. (Figure 7c). We infer that the mass flow was mainly oriented southward, and as the paleo-slope gradually turns gentler, it then spreads towards the southeast and southwest. This suggestion is also supported by the characteristic of hummock density

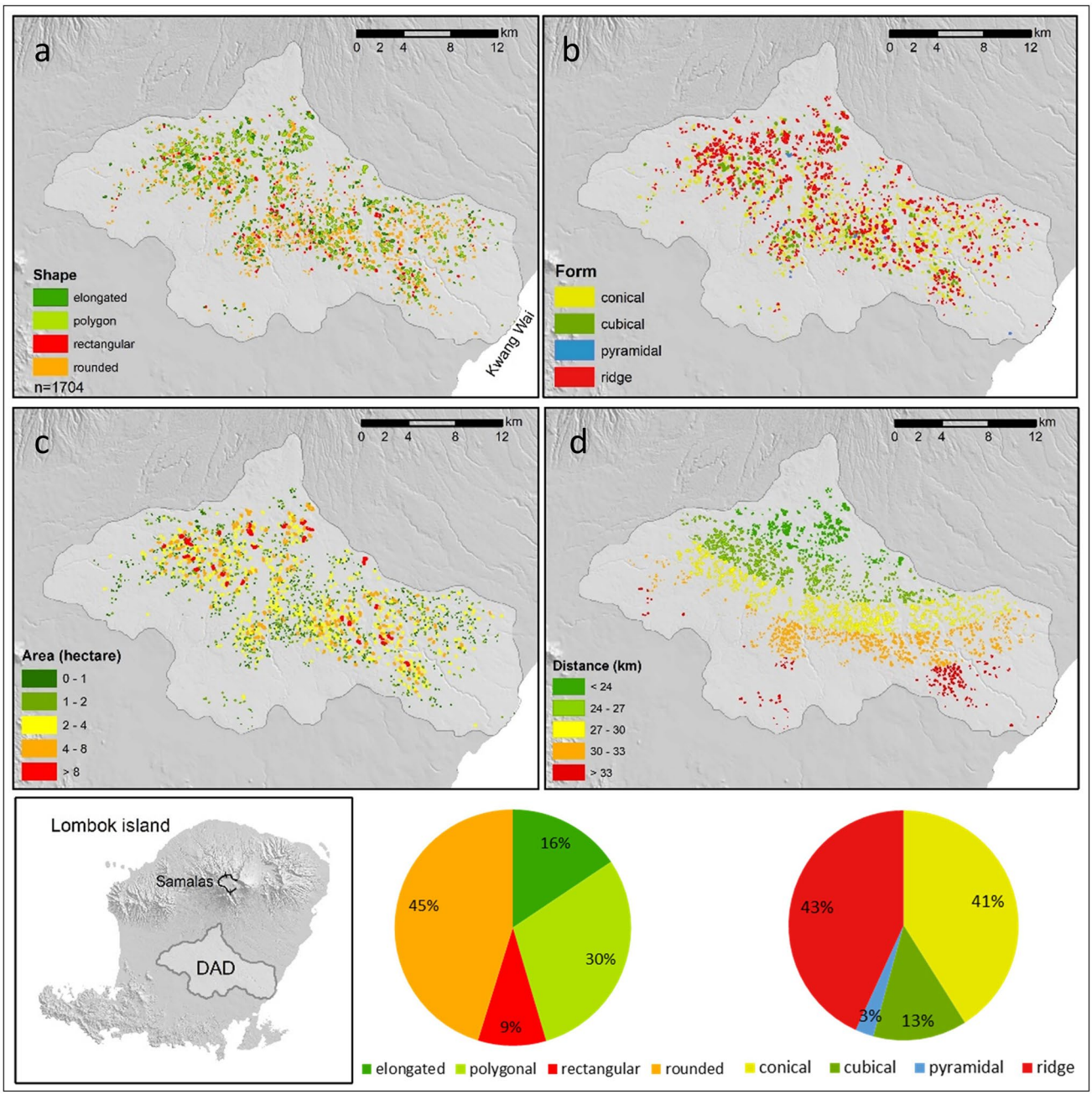


**Fig. 5** Map of morphological characteristics of individual hummocks: shape (**a**), form (**b**), area (**c**), distance (**d**). Pie charts indicate the percentage of hummock shape (left) and hummock form (right)

that clustered in the middle-south area (Fig. 7d). This area is proposed as the centroid of the DAD, where the distribution of hummocks is the densest (18/km$^2$, with an average of 3/km$^2$)

Three main domains of the DAD can be distinguished: toreva, hummock, and piedmont (Fig. 8a). Toreva occupies a small part of the upper area of the DAD with ~3 km along a linear transect (Fig. 8b). The hummock domain is the largest unit in the DAD of Samalas with ~18 km span. The piedmont domain is smaller, covering ~5 km long in the distal part of DAD. Two colluvial fans have been identified in the southern area, characterized by redelivery of debris avalanche deposits, involving mass wasting and fluvial transport. Other profile lines in the W-E (line CD) and the N-S (line EF) directions show the configuration of the densest area of the hummock. In both topographic profiles, "h" marks the peak of each hummock. On the profile CD (Fig. 8c), nine hummocks

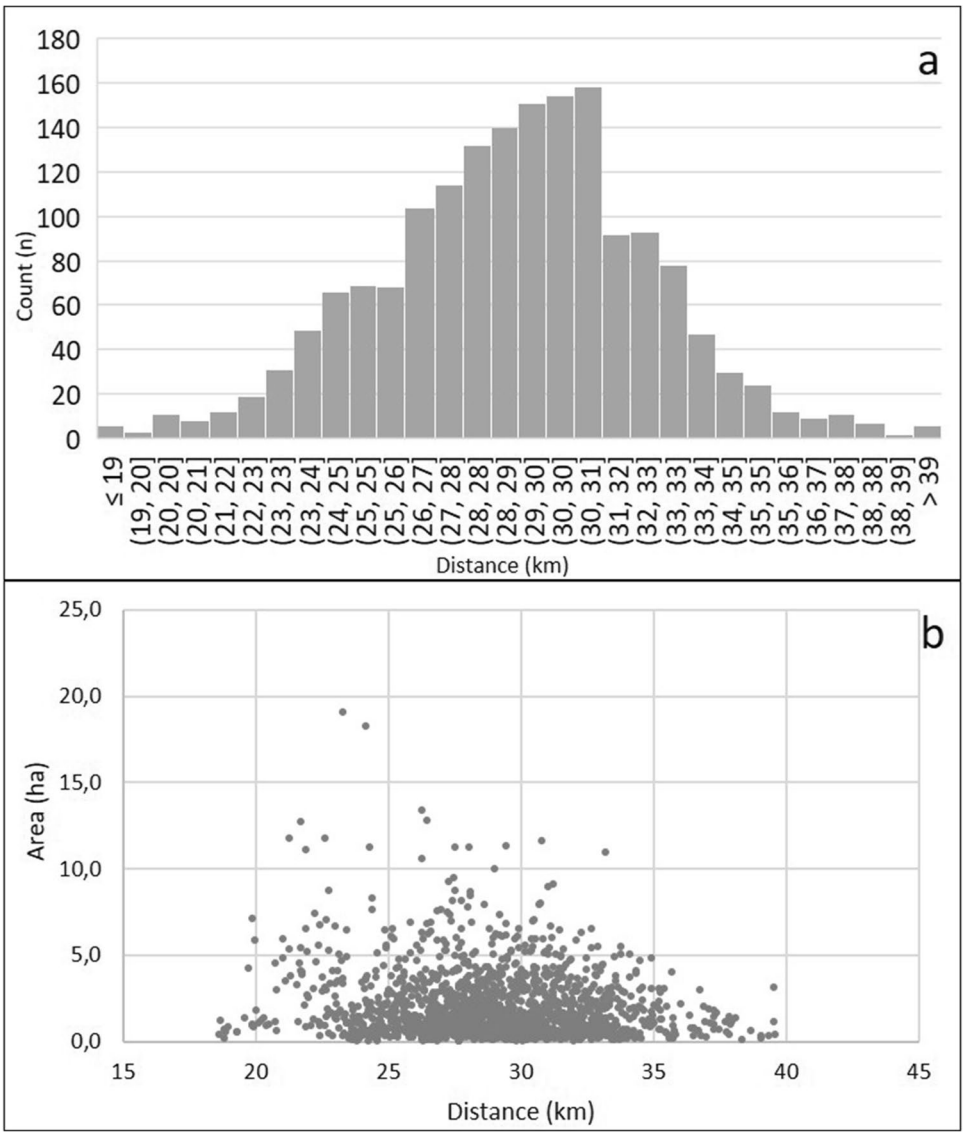


**Fig. 6** Histogram of hummocks distribution (**a**) and chart of area vs. distance from the source (**b**)

have been identified, with an average distance of 350 m between each. A wider space separates hummocks on profile EF (Fig. 8d), with an average of 450 m between identified hummocks. Across both profiles, most hummocks are 7 m high and can reach a maximum of 20 m.

Hummock trains (HTs) are distributed in the middle and lower parts of the hummock domain. HTs in Kalibabak DAD generally point three directions: the west part indicates a southwesterly direction, the central part indicates a southerly direction, and the eastern part indicates a southeasterly direction. The extension of the HTs (dark-brown arrows in Fig. 8a) can be used to portray the possible direction of the avalanche flow. Other morphological characteristics, such as aspect and hummock density, have also supported this suggested flow direction.

## Structure of DAD

Two types of deposits were found along the river channels: (a) large boulder and (b) blocky-matrix textures. In the middle stream of the Kali Palung river (26 km from the caldera rim, Fig. 9a), large boulders are scattered along the river channel. These large boulders, visible at low water-stage, are the result of erosion processes along the Kali Palung valley. In the distal part of the DAD, 35 km from the caldera rim, rivers are dominated by boulders of a smaller size mixed with a sandy matrix (e.g., in the Perampung river). On this DAD deposit, fluvial material composed of sandy silt covers the DAD layer (Fig. 9b). In another part of the Kali Palung valley, 35 km from the caldera, the DAD has a blocky texture with occasional boulder-sized blocks and is up to 10 m thick

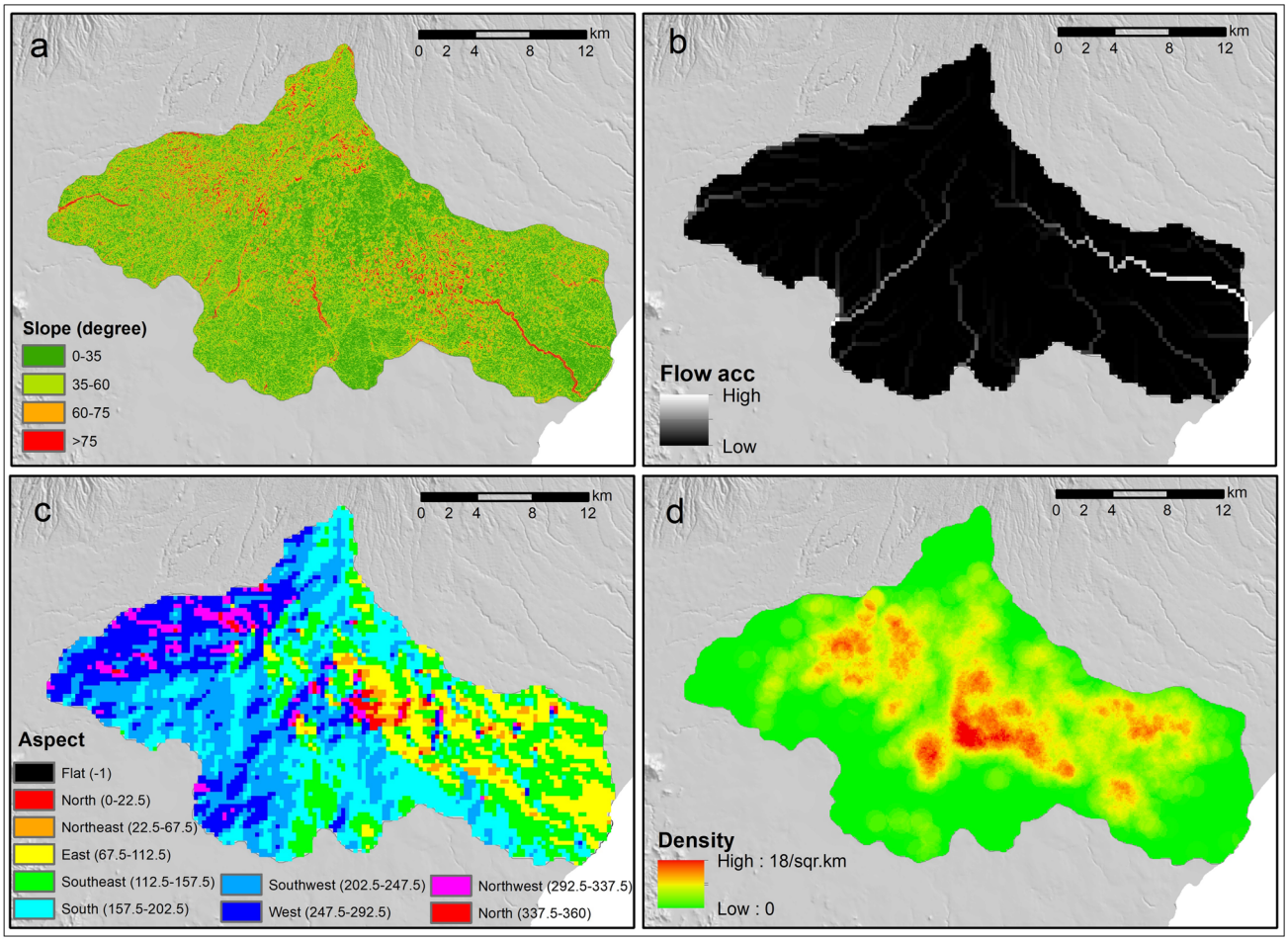


**Fig. 7** Map of morphological characteristics of DAD: slope (**a**), flow accumulation (**b**), aspect (**c**), hummock density (**d**)

(Fig. 9c). Here, the DAD is in direct contact with an older weathered layer, identified as a calcareous breccia formation called Kali Palung (Mangga et al. 1994).

Twenty-nine kilometers to the south of the caldera rim, nearly homogeneous DAD structures can be observed, with sheeted lava (Fig. 9d) including jigsaw cracks (Fig. 9e). Another hummock located at 28 km south of the caldera rim, has a matrix comprising 75% sand. Many medium boulders are also visible, along with meter-sized boulders (Fig. 9f). In this sector of the flank, no pyroclastic material from recent eruptions of Samalas could be observed, while in the southwestern sector, 23 km from the caldera rim, a mantle of pumice-fall from the 1257 CE Samalas eruption can be observed. In locations where the pumice layers were found, a relatively thick (~1.5 m) paleosol developed in between the Samalas 1257 CE eruption and the DAD, showing that the two events were not concomitant (Fig. 9g).

Completing the outcrop observations, 10 cores were collected from ESDM (Fig. 10). Based on these data, the lithological type of the DAD was confirmed as a mixture of breccia, lava, boulders, and consolidated tuff-gravelly sand, overlain by recent soil of variable thickness. The formations underneath the DAD have similar characteristics in most cores, characterised by weathered tuff-lapilli, calcareous breccia, and gravelly sand with boulders, and can be linked to the Kali Palung rock formation (Geological Map; Mangga et al. 1994). The minimum thickness (12 m) of the DAD is located at the Janapria core (Fig. 10a), and the maximum thickness (58 m) is found from the Peresak Daye core (Fig. 10b), and from the Suwangi core (55m). Correlation between cores in the NS direction (Jenggik-Janapria) shows that the DAD thickness significantly decreases according to the flow direction (Fig. 10a), whereas in the WE direction (Sapit-Tanak Kaken), the DAD's thickness increases in the center and decreases towards the margins (Fig. 10b).

To provide an overview of the internal structure of DAD that is not covered by core or outcrop data, 2D electric resistivity transects were acquired at Lepak, East Lombok, and are 550 m long each, providing a spatial window on the deposit (Fig. 11). The DAD in Lombok is characterized by resistivity values in the range of 30-300 ohm-m, defined from the resistivity measurements that are referenced to the

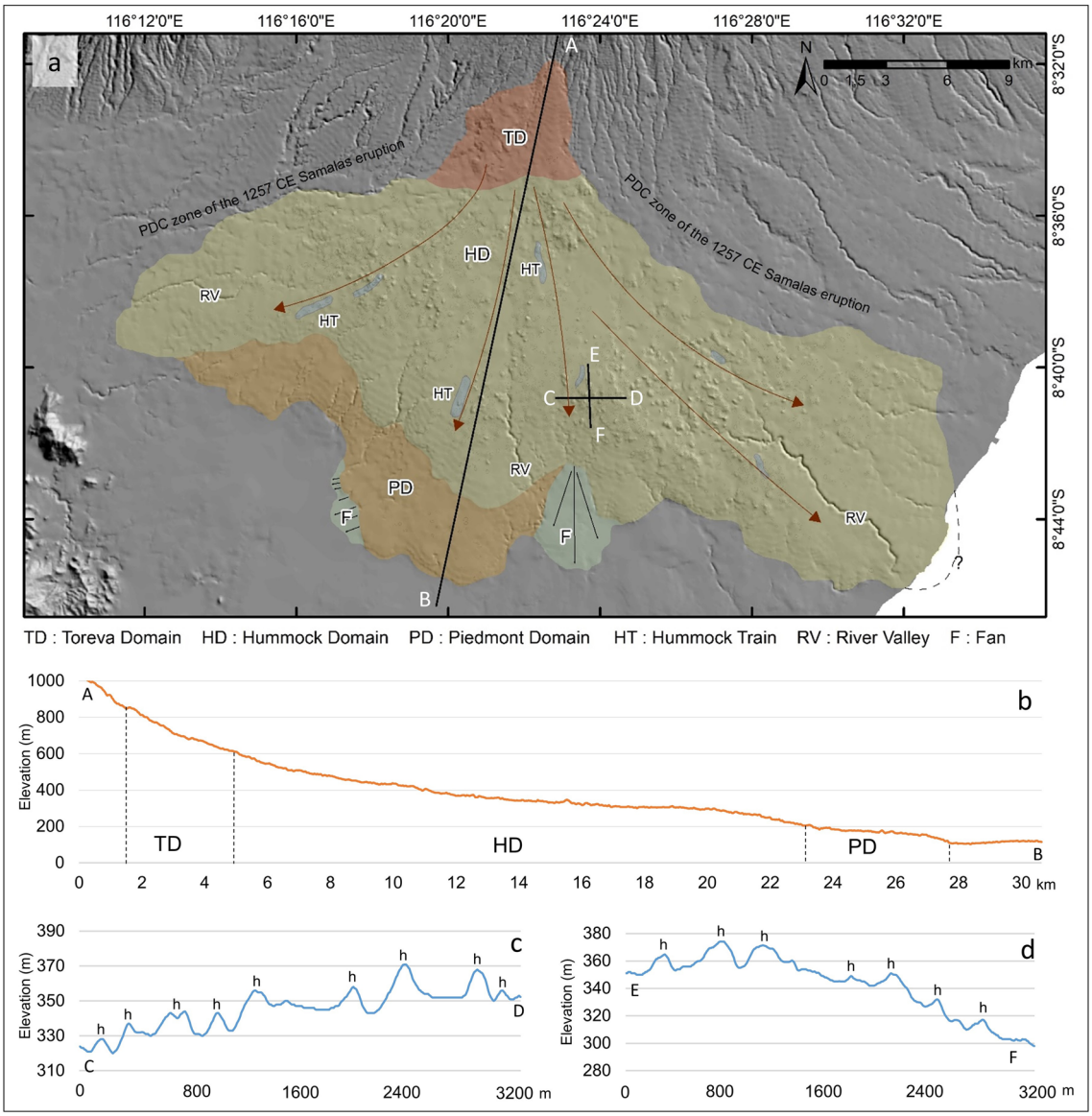


**Fig. 8** Map of the DAD extent in Lombok, (**a**) showing the delineation of DAD domain and suggested mass flow directions. (**b**) Profile line AB displays the topography from upper to lower area of DAD along N-S axis. Sudden break of slope indicates the boundary of DAD area. Profile lines CD (**c**) and EF (**d**) in the densest area of hummock indicate the configuration of peak, valley, and flat areas of hummocks

Janapria and Jenggik cores. Two measured lines AB and CD show that the DAD layer has contrasting boundaries with the basal material, which has a lower resistivity value (a small value indicates a high-water content or highly saturated layer). The boundary between the DAD and older material along the line AB forms a continuous boundary (black line) at a depth of 20-30 m. The upper layer of the line AB displays two layers of low resistivity that can be interpreted as a fluvial deposit covering the DAD. A chopped hummock due to anthropogenic activity is also identified at a distance of 250-370 m from point A (Fig. 11). On the line CD, the limit of the DAD is more irregular in depth, indicating either that (1) the paleo-topography is irregular, or (2) the DAD has eroded the paleo-topography. The paleo-topography of this location may be composed of weak materials that are not resistant to erosion. Similar to the line AB, small fluvial infills are also found on the line CD. Other resistivity measurements in various locations of the DAD are presented in the Supplementary Material (Table S1).

## Paleo-topography

Field observations combined with DEM data were used to reconstruct the pre-collapse topography of Samalas volcano

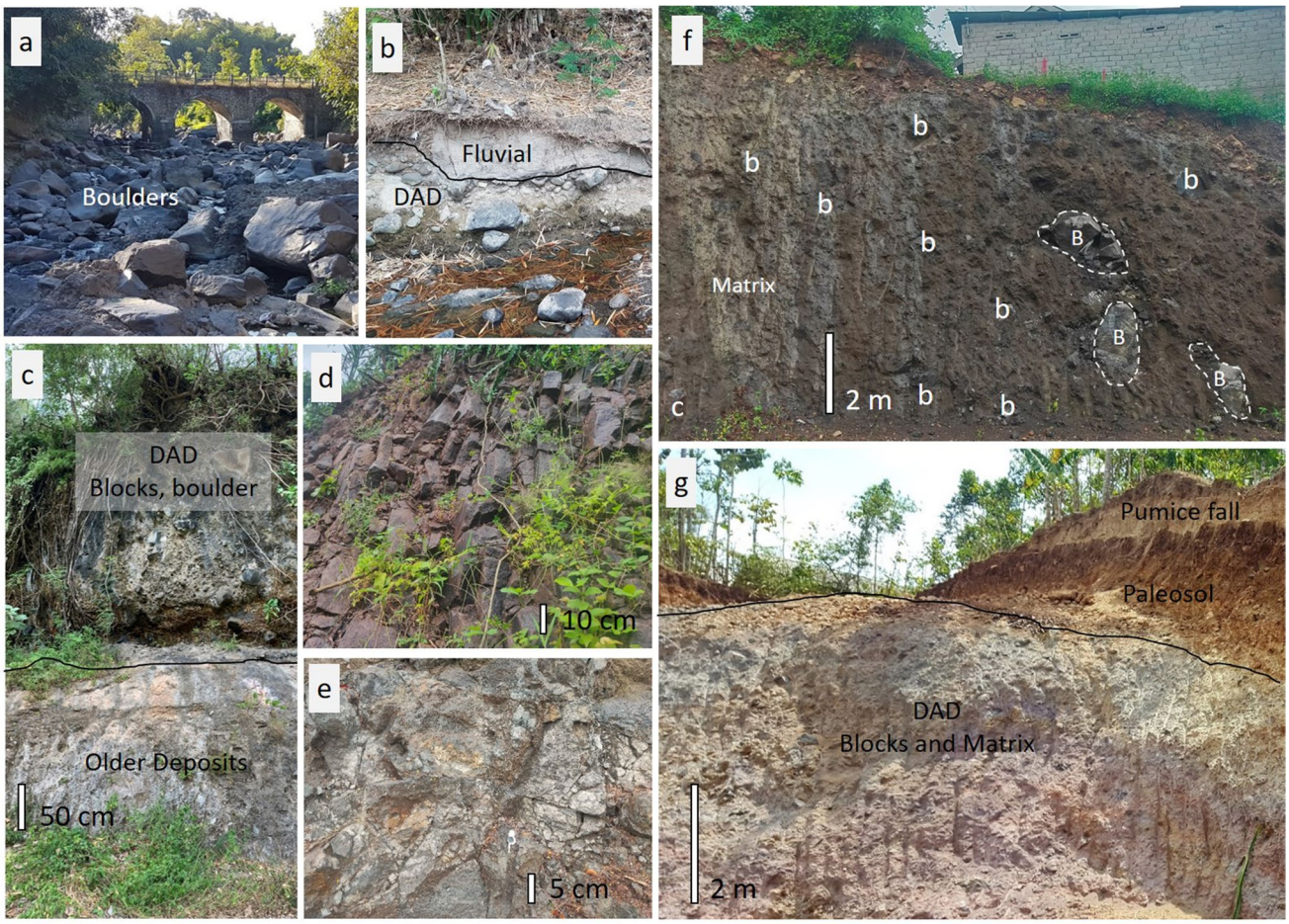


**Fig. 9** Structure of the DA in various locations. **a** Scattered boulders along the river channel in the middle stream of Kali Palung. **b** DAD covered by fluvial deposits in Perampung riverbanks. **c** Blocky texture dominating an escarpment in the Kali Palung valley. Sheeted lava **d** with jigsaw cracks **e** observed in an opencut hummock. **f** Opencut hummock composed of blocky texture "b", boulders "B", and matrix. **g** Complex outcrop in the western part of the study area that records pumice fall deposit from the 1257 CE eruption, paleosol, and DAD facies (boulder and matrix)

(Fig. 12a). Based on our morphological reconstruction, the pre-avalanche summit was located at ~3.6 km from the current summit of Rinjani and adjacent to the current Barujari vent (~500 m). The reconstructed summit cone has an average slope of 35%. In comparison to the Rinjani crater, the Samalas has a larger circular body (Fig. 12a). Best estimation using ShapeVolc indicates that former (pre-avalanche) Samalas has a maximum height of 4207 m, higher ~480 m than the current Rinjani. The topographic profile A-B (Fig. 12b) of the DAD demonstrates that the stratocone of the former Samalas was ~1,500 m higher than the caldera rim. The pre-avalanche and the present topographic profiles intersect at ~8 km from the simulated former summit. According to the reconstructed profile line, the possible collapsed edifice that released the debris avalanche has a maximum length of ~8 km and an average depth of ~1.5 km (Fig. 12b: blue-shaded area). These dimensions provide the maximum constraint of the collapsed volcanic sector that produced the Kalibabak debris avalanche. Therefore, the size of the horseshoe scar is smaller than those estimated length and depth.

## Metrics of the DAD

Based on the calculated metrics (Table 2), the length ($L_D$) of the DAD is smaller than its width ($W_D$), displaying a stretching-fan shape. The thickness of the DAD was then calculated to be approximately 28.5 m on average. According to the classic geometrical formula (Table 2), the volume of the DAD can be estimated to be 15.3 $km^3$, which compares well with the DEM subtraction method, which yields 14.9 $km^3$, or 15.1 ± 0.5 $km^3$ if we average both results and apply the estimated uncertainty. The measurements also show that the tail of the flow is at 685 m a.s.l., while the front traveled to a final altitude of 114 m a.s.l. This gives an $H_D$ value of 581 m. By comparing $H_D$ and

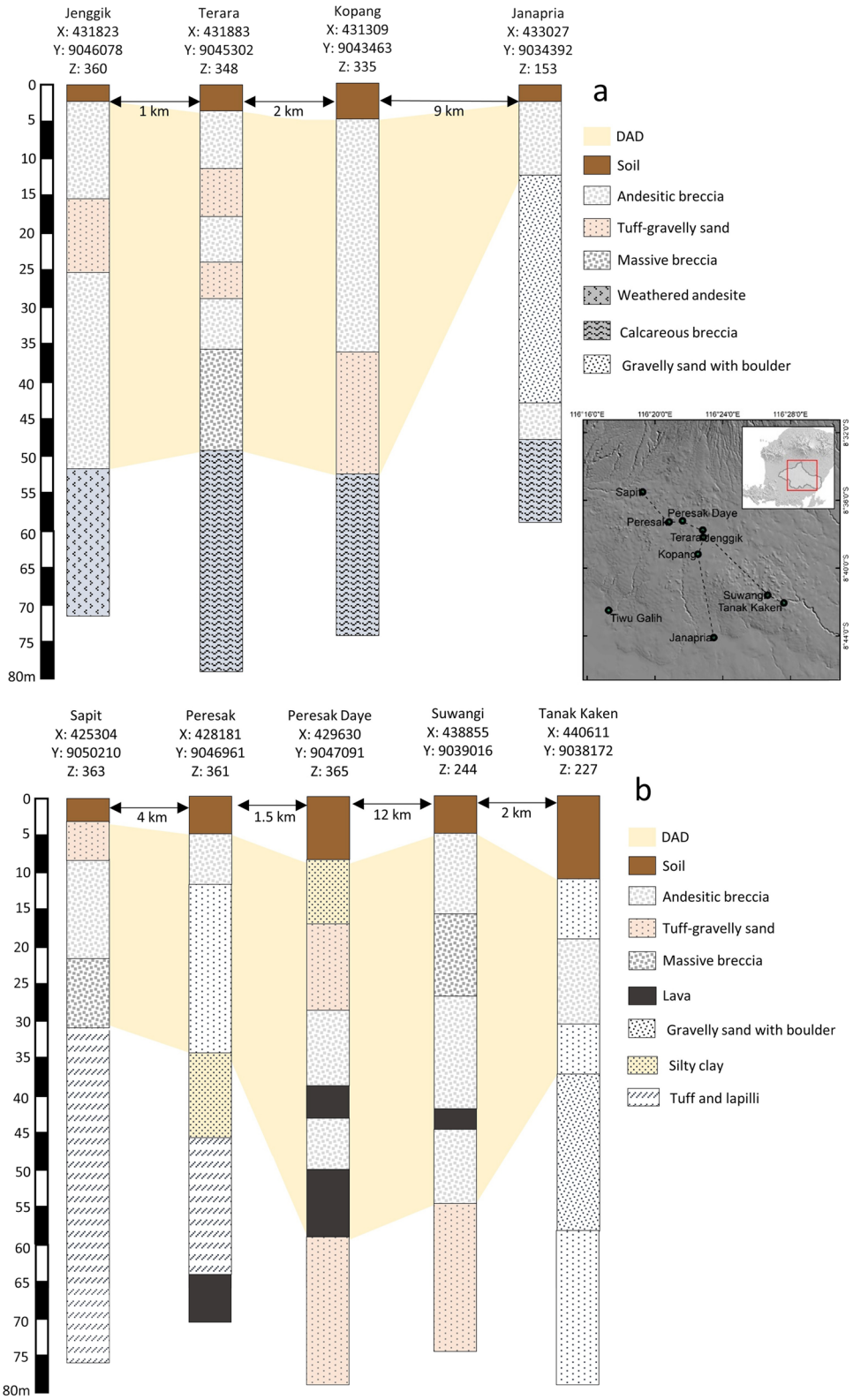


**Fig. 10** Lithological information of the DAD from sediment core data. Correlations between deposits associated with the DAD demonstrate the variety of thicknesses

$L_D$ values, we get an average slope of 2%. Although the overall slope has been mapped (Fig. 7a), this metric is important for characterizing DAD in Lombok that can be used for comparison with other DADs. The length (L) of the debris avalanche from the source to the front is 39.3 km, with a maximum drop height of 4 km. Comparison of these two metrics results in the H/L value of debris avalanche in Lombok being 0.1.

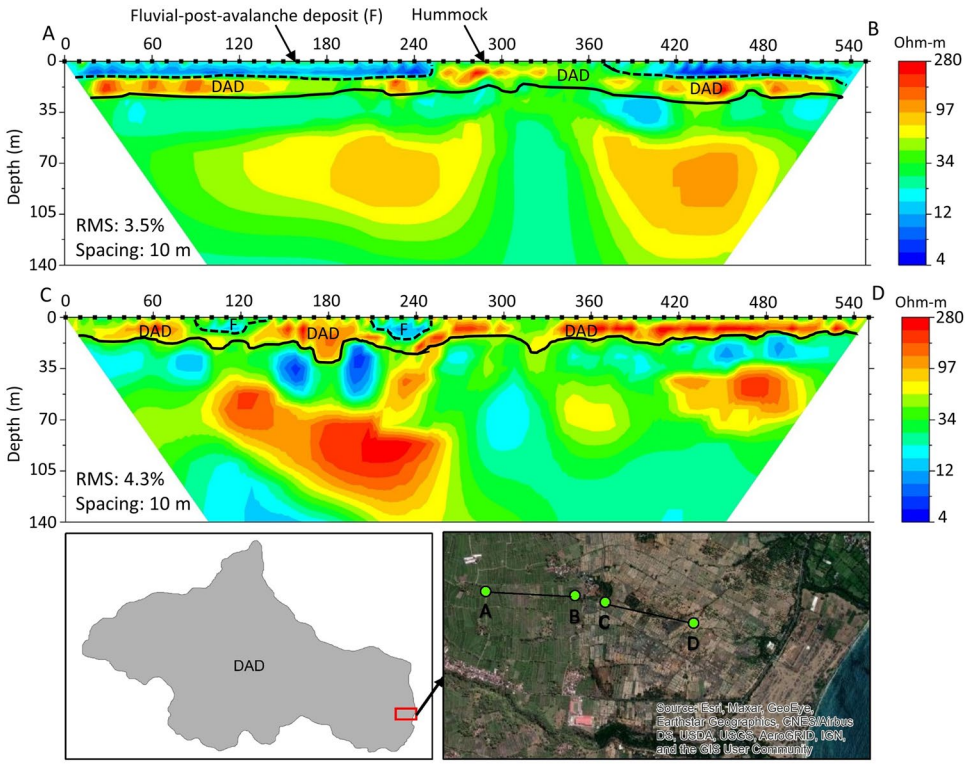


**Fig. 11** Interpretation of the resistivity profiles in the eastern part of DAD

## Modeling of the Debris Avalanche

The debris avalanche was further simulated using VolcFlow. We conducted four simulations to evaluate the debris avalanche propagation from Samalas volcano (Supplementary Material: Table S2). The first simulation used a volume of ~15 $km^3$ and a yield strength of 50 kPa to determine the avalanche propagation and area of coverage for a dense material. Results show that the simulated deposition poorly matches the actual deposit (Fig. 13a). However, the maximum deposit depth of this simulation (60 m) is nearly similar to the maximum measured depth from the outcrop (58 m).

The second simulation was conducted with the same volume with moderate yield strength (20 kPa). The result of this simulation has further and broader coverage but did not reach the most distal part of the deposit (Fig. 13b). The third simulation used a lower value of yield strength (7 kPa), indicating a less compacted material. The result of the third simulation is most similar to the original DAD in shape and coverage (Fig. 13c). In the distal southern part, the front limit is relatively similar, as well as in the southeastern part, where the avalanche reached the coastline.

The last simulation used a standard yield strength that is generally applied for simulating DAD propagation, which is 50 kPa, similar to the first simulation. However, this simulation used double the calculated volume (i.e., ~30 $km^3$). The result shows that the final propagation of DAD reaches the outer boundary of the original DAD, although the final form is not identical (Fig. 13d). The resulting maximum deposit thickness also reached twice the measured maximum DAD depth. Based on this fourth simulation, it can be assumed that the Kalibabak DAD may be characterized by lower yield strength. The simulation might be more accurate if the scar of the caldera avalanche is visible since the volume between the caldera avalanche and the deposit can be compared, as well as the starting point of the emplaced material can be determined.

## Age of Debris Avalanche

The results of radiocarbon dating of the soil between the DAD and the 1257 eruptive material display ages ranging from 2,600 BCE to 1,300 BCE, with one younger date of 464 CE (Table 3). This supports the thesis that the DAD is much older than the Samalas 1257 CE eruption. The oldest age constraint of the Kalibabak DAD is determined based on the dated material below the DAD. The results are more diversified, with a range of ~10,000 years. The oldest calibrated age obtained from a paleosol in the Kali Dalam Valley is 17,935 BCE. Nearby, in the same valley, another paleosol sample yielded a calibrated age of 15,790 BCE. A sample from Kali Palung, which has a similar stratigraphic sequence to Kali Dalam, but is located in the distal part of the DAD, yielded a calibrated age of 11,495 BCE. At Kwang Wai beach, in the edge (front) of the DAD, two materials below the coastal hummock yielded a calibrated

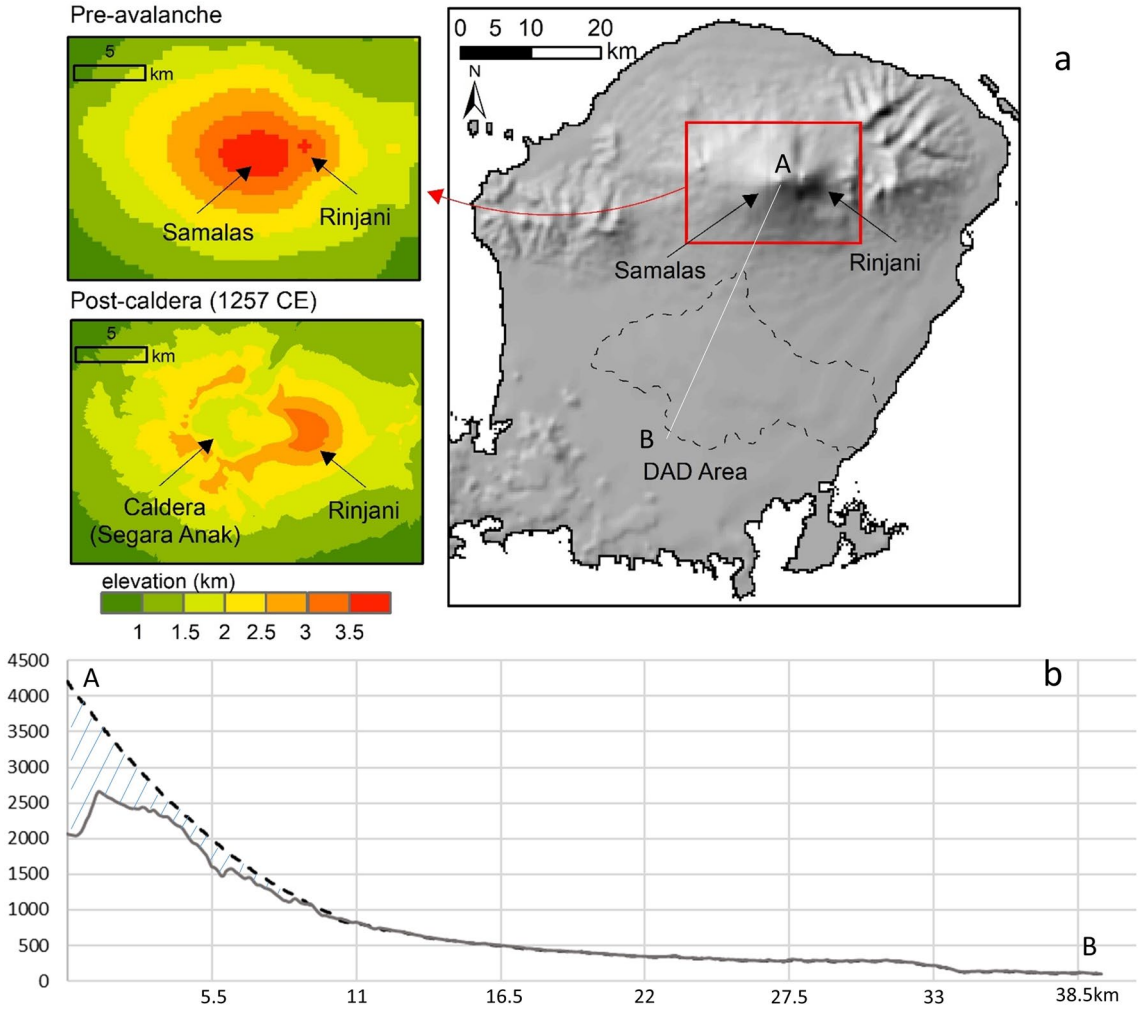


**Fig. 12** **a** Comparison of the paleo- and present-day DEMs of the Samalas summit. **b** Profile line from the summit to the distal area shows topographic differences between the paleo- and present-topography

**Table 2** Metrics of the Kalibabak debris avalanche from Samalas volcano, Lombok

| No | Parameter | Value |
|---|---|---|
| 1 | $L_D$ (km) | 25 |
| 2 | $W_D$ (km) | 41 |
| 3 | $A_D$ (km$^2$) | 535.7 |
| 4 | $H_D$ (m) | 581 |
| 5 | $<_D$ (%) | 2 |
| 6 | $T_D$ (m) | 28.5 |
| 7 | $V_D$ (km$^3$) | 15.1 ± 0.5 |
| 8 | $AR_D$ | 2.1 |
| 9 | L (km) | 39 |
| 10 | H (km) | 4.1 |
| 11 | H/L | 0.10 |

age of 7,000-7,600 BCE. At this site, the exposed seafloor (KW2) is dated at 10,158 BCE. Located closer to the caldera rim (27 km), the paleosol covered by the DAD at Kali Dalam may have undergone significant erosion during the flow; therefore, the sampled paleosol is likely much older than the avalanche event. In contrast, the exposed materials beneath the DAD at Kali Palung and Kwang Wai beach, which are located 34 km and 39 km from the caldera rim respectively, are much younger because erosion may have decreased. Based on our dating of the paleosols above and below the DAD, the age of the Kalibabak DAD is estimated within the range 7,000 and 2,600 BCE.

## Discussion

### A gigantic debris avalanche in Indonesia

A previous study reported that at least 70 volcanic sector collapses were identified in Indonesia (MacLeod 1989). Since these data were developed by the interpretation of

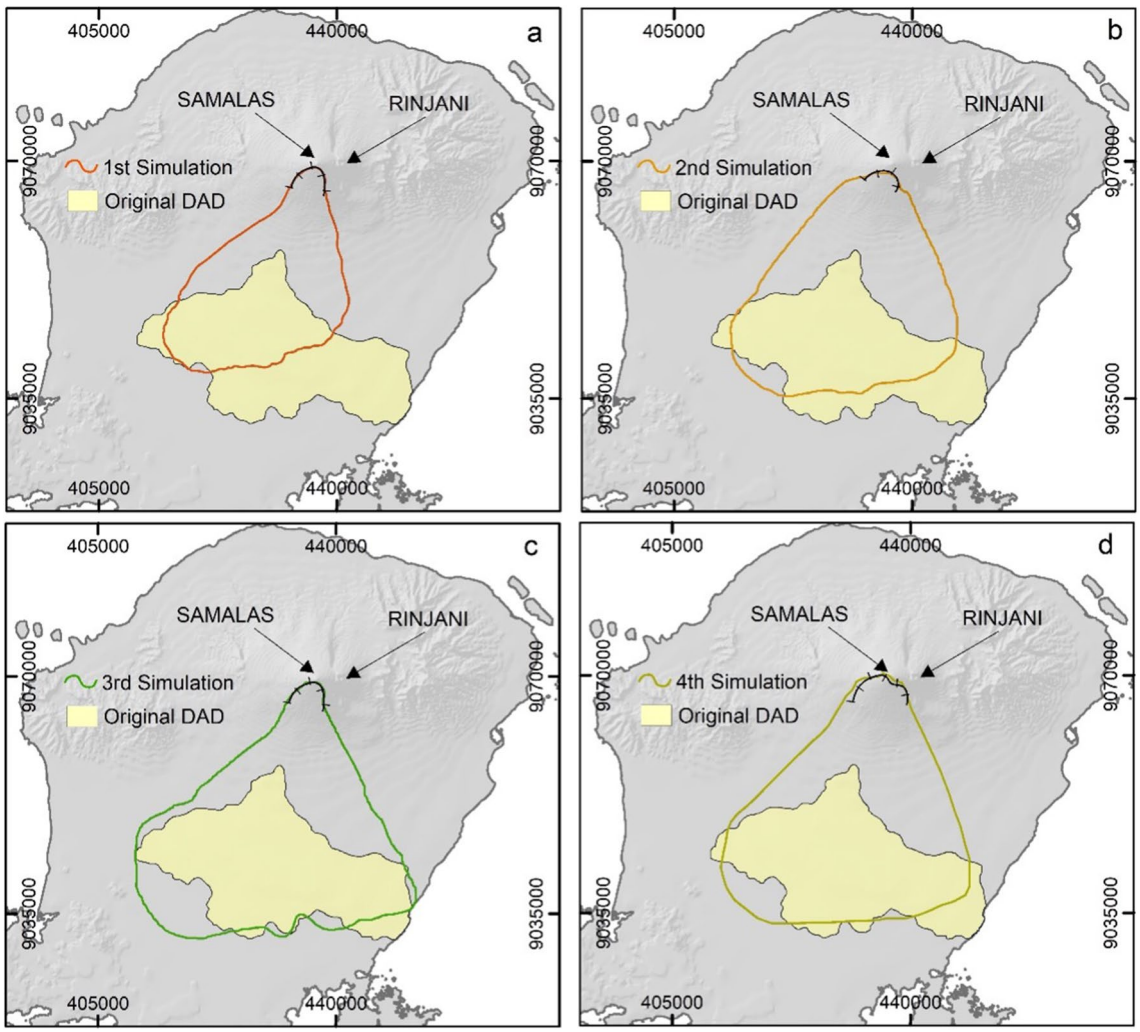


**Fig. 13** Comparison of the simulated and original DADs; ~ 15 $km^3$ and 50 kPa (**a**); ~ 15 $km^3$ and 20 kPa (**b**); ~ 15 $km^3$ and 7 kPa (**c**); ~ 30 $km.^3$ and 50 kPa (**d**)

**Table 3** Radiocarbon ages of the paleosols and sediments related to the Kalibabak DAD

| No | Site | Type | Age BP | Calibrated age (BCE) | Median probability (BCE) |
|---|---|---|---|---|---|
| 1 | Selebung (DAD 1) | Paleosol above DAD | 3,080 ± 30 | 1,413–1,254 | 1,326 |
| 2 | Selebung (DAD 2) | Paleosol above DAD | 4,100 ± 50 | 2,708–2,474 | 2,647 |
| 3 | Selebung (DAD 3) | Paleosol above DAD | 3,120 ± 50 | 1,456–1,222 | 1,352 |
| 4 | Selebung (DAD 4) | Paleosol above DAD | 1,635 ± 30 | 404–540 (CE) | 464 (CE) |
| 5 | Kali Dalam 1 (KD1) | Paleosol below DAD | 14,490 ± 60 | 15,826–15,540 | 15,790 |
| 6 | Kali Dalam 2 (KD2) | Paleosol below DAD | 16,490 ± 50 | 18,052–17,874 | 17,935 |
| 7 | Kali Palung (KP) | Detritus sediment | 11,580 ± 230 | 11,938–11,118 | 11,495 |
| 8 | Kwang wai 1 (KW1) | Paleosol below DAD | 8,620 ± 330 | 8,020–7,339 | 7,699 |
| 9 | Kwang wai 2 (KW2) | Compacted detrital sediment | 10,380 ± 300 | 10,836–9,274 | 10,158 |
| 10 | Kwang wai 3 (KW3) | Paleosol below DAD | 8070 ± 500 | 8,251–5,986 | 7,029 |

aerial imagery, 54 were considered probable events, while the remaining 16 were possible events. These numbers are used to rank Indonesia in the global inventory of volcanic debris avalanches (Dufresne et al. 2021). However, only 11 DADs from this list have been subjected to morphometric measurements, and only four were successfully dated, e.g., Galunggung, Papandayan, Raung, and Ili Werung (Siebert et al. 1987). Our work provides a new case study to add the current database. In Indonesia, most DAD volumes vary from 1 to 5 $km^3$, with an area of 50-250 $km^2$ (MacLeod 1989). The largest known DAD in Indonesia is located at the foot of Raung volcano in East Java, with a travel distance up to ~80 km, and an area of ~650 $km^2$ (Siebert 1984; MacLeod 1989). Based on the inventoried data, the Kalibabak DAD (~15 $km^3$) ranks third in Indonesia in terms of volume, below the DAD from Raung (25 $km^3$) and Galunggung (16 $km^3$) (Siebert 2002).

To determine its position at a global scale, the metrics of DAD in Lombok need to be compared with other DADs worldwide. In the East Asian region, Japan is among the countries with the largest number of DADs (Ui et al. 1986; Siebert et al. 1987). From all the debris avalanches that have occurred in Japan, no significant DAD has a volume of >10 $km^3$, and the farthest travel distance (L) reaches 32 km. Similarly, compared to the Philippines, New Zealand, Melanesia, and Kuriles-Kamachatka regions, the Kalibabak DAD is significantly bigger than all DADs in those regions. In Europe, a Holocene debris avalanche on the eastern flank of Etna volcano, known as the Valle del Bove DAD, has roughly the same volume as the DAD at Samalas volcano (~14 $km^3$) (Calvari et al. 2004). However, several Holocene DADs worldwide are comparable in volume to the one produced by Samalas, e.g., Meru, Tanzania (10-20 $km^3$), Fuego, Guatemala (15 $km^3$), and Antuco, Chile (15 $km^3$) (Siebert 2002). Based on this inventory (Siebert 2002), the Kalibabak DAD from Samalas volcano ranks eighth among the largest (>5 $km^3$) Holocene DADs worldwide.

## Triggering mechanism and dating of the event

Identification of the triggering factors that cause a volcanic collapse is challenging, especially when it occurred in the past and when no direct observations are available (Özdemir et al. 2016; Valverde et al. 2021). Several factors can trigger a collapse of a volcano, such as earthquake or fault activity, volcanic eruption, or dyke intrusion (Tibaldi 2001; Belousov et al. 2007). It can be triggered by single or multiple factors. There are no fault lines beneath the Rinjani volcanic complex that are likely to cause significant earthquakes (Fig. 1b). The major earthquake source zones are located in the north (Flores Thrust) and south of Lombok (Indo-Australian subduction) (Harsuko et al. 2020). A series of recent earthquakes in the northern region of Lombok Island in 2018 (6.9 Mw) caused significant damages and landslides in Lombok. Identification using satellite images provided data of 9,319 minor landslides with a total area of 10.39 $km^2$, predominantly located in the mountainous areas (Ferrario 2019). Although the epicenter is located on the northern slope of the Samalas-Rinjani complex and has affected ground deformation, the volcanic activity in Samalas-Rinjani remains normal without significant escalation (Wibowo et al. 2021) (Wibowo et al. 2021). Earthquakes and fault activity may be possible triggering factors in other locations, but not for a large volcanic avalanche in Lombok.

The regional stratigraphic frameworks that have been established (Nasution et al. 2004; Vidal et al. 2015; Métrich et al. 2017) can be used as benchmarks for establishing the relationship between eruptions and the Kalibabak DAD (Fig. 14). Correlation between the age of DAD and stratigraphic framework was also demonstrated in Shiveluch volcano (Russia) to determine the association between debris avalanches and eruptive events (Belousov et al. 1999; Ponomareva et al. 1998). Holocene activity in the Rinjani-Samalas complex was dominated by basaltic explosive activity that produced scoria fall and PDC deposits between 11,000 and 5,300 BCE. Large explosive eruptions were absent during this period. The subsequent period (~5,300-800 BCE) was characterized by effusive and explosive volcanic events. For example, the Rinjani volcano expelled the Lembar trachy-dacite lava flow. Scoria fall, which is a typical product of explosive basaltic eruption, were also identified on the northern slope of Samalas. The radiocarbon dating of two charcoals in this deposit yielded 4,700-5,000 BCE (Métrich et al. 2017). Lastly, a younger pumice deposit overlying the scoria fall deposit, i.e., the Propok pumice, was dated between ~5,000 and 800 BCE (Nasution et al. 2004; Métrich et al. 2017). It was ejected eastward during an assumed sub-Plinian eruption of Samalas, with an estimated volume of 0.1 $km^3$ (dense rock equivalent-DRE) (Nasution et al. 2004).

Based on the age range of the DAD (7,000–2,600 BCE) obtained from our radiocarbon dating (Table 3), we argue that the debris avalanche event was likely triggered by the eruptive event that expelled the Propok pumice. To determine a more precise age of the Propok pumice, we obtained four additional dating from two outcrops on the northeast slope of Samalas-Rinjani consisting of three paleosols below and above the pumice deposits, as well as a charcoal within 70 cm thick pumiceous PDC layer (Table 4). These outcrops are on the same slope segment, one on the upper side (BBG) and the other on the lower side near the break of slope (BB) (Supplementary Material: Figure S2). The paleosol below the pumice layer and the charcoal within the PDC deposit yield an age of 3,506-3,430 BCE and 3,637-3,508 BCE, respectively. Considering that (i) these ages fall within the range of those attributed to the Propok pumice, and (ii) the thickness of the deposit falls within the isopach of the same

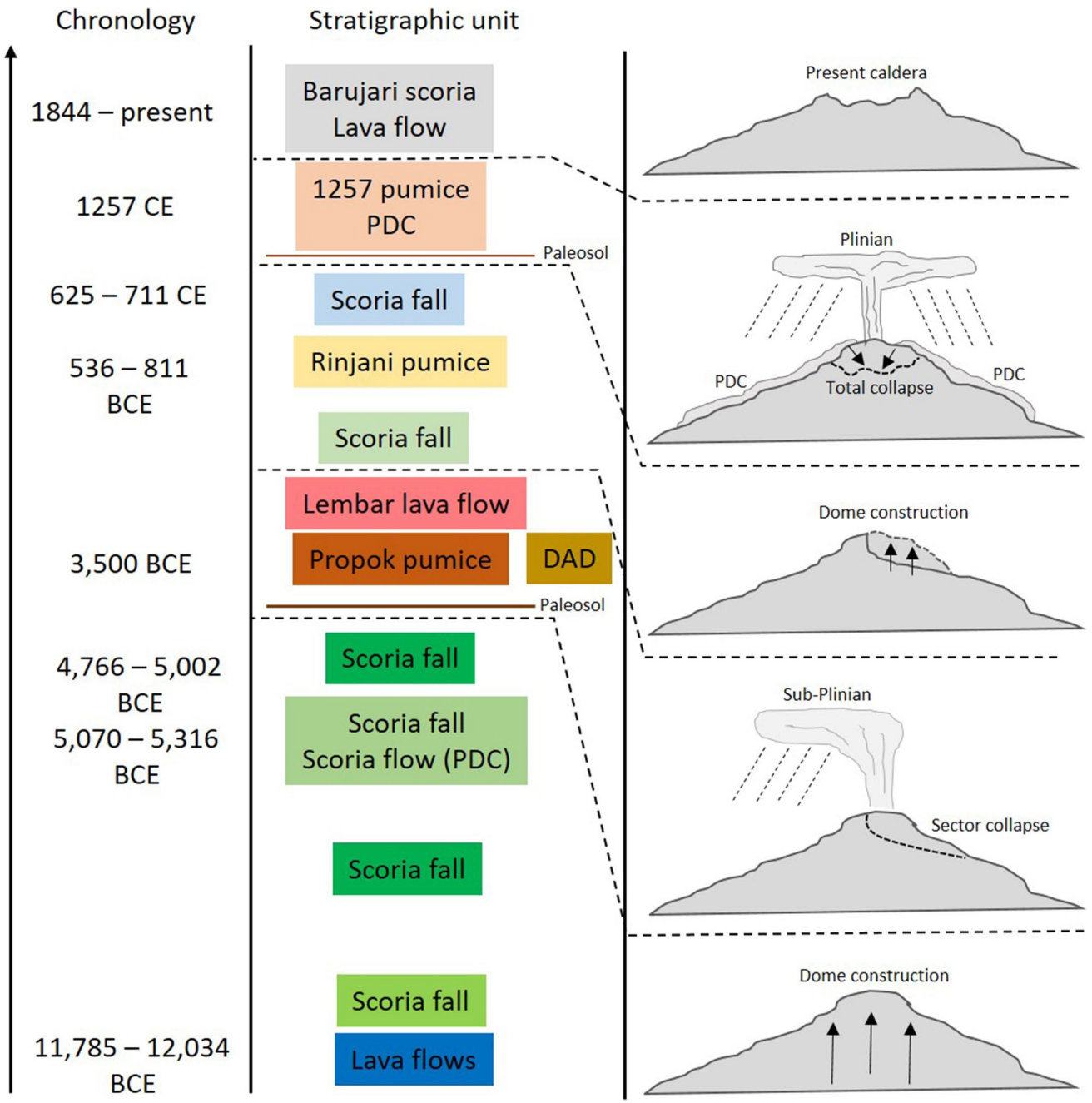


**Fig. 14** Stratigraphic framework and chronology of the landscape dynamics in Samalas volcano

**Table 4** Radiocarbon ages of the paleosols and charcoal related to the Propok pumice

| No | Site | Type | Age BP | Calibrated age (BCE) | Median probability (BCE) |
|---|---|---|---|---|---|
| 1 | Bumbu 1 (BB 1) | Paleosol below Propok | 4,676 ± 24 | 3,506–3,430 | 3,454 |
| 2 | Bumbu 3 (BB 3) | Paleosol above Propok | 4,417 ± 28 | 3,102–2,911 | 3,014 |
| 3 | Bumbung 1 (BBG 1) | Paleosol | 5,799 ± 28 | 4,714–4,544 | 4,635 |
| 4 | Bumbung 2 (BBG 2) | Charcoal | 4,779 ± 31 | 3,637–3,508 | 3,570 |

eruption, we infer that the Propok pumice and the associated debris avalanche occurred ca. 3,500 BCE (Fig. 14).

## Emplacement Dynamics

The long runout distance of the Kalibabak debris avalanche deposit is not due to the massive presence of water or a lahar-transform mechanism. The unusual runout distance of 39 km, with a H/L ratio of 0.1, is predominantly caused by the intense rock fragmentation in the deposit. This H/L ratio is placed near to Chimborazo and Meru (Fig. 15a). In the case of Kalibabak DAD, the rock fragmentation process is a significant factor in the peculiar and long runout mass distribution. Rock fragmentation produces high-speed fragments moving in all directions, which generate isotropic dispersive stress within the moving mass, as indicated by the jigsaw crack in the deposit (Davies et al. 1999). However, a longitudinal dispersive stress acts in the direction of reducing the mass depth. As a result, the rear part of the moving mass tends to decelerate, and contrary, the front of the moving mass tends to accelerate (Davies et al. 1999).

The comparison of the four simulations with the original boundary of the DAD suggests that the Kalibabak debris avalanche is complex to simulate. However, VolcFlow models assisted in better understanding the dynamics of DAD emplacement in Lombok. The third simulation may be the best approximation (Fig. 13c). However, field conditions indicate that the structure of the DAD is not composed of fluid materials such as lahars or highly saturated materials. Therefore, we suspect that two sequences occurred during the DAD emplacement (Fig. 15b); Zone I is freely spreading material emplacement type, while Zone II is channelised or valley-filling (Yoshida 2014). The simulation also demonstrates that the area of original deposit may be bigger than the actual delineated boundary. The intersection area between the simulated DADs and the original DAD could be suggested as part of Kalibabak DAD. This area is occupied by material that remained near the source, which may be in the form of toreva or slumped blocks. However, due to the enormous PDCs in 1257 CE and the subsequent lahars, this area was buried and is not visible as a DAD area. The predicted avalanche caldera at Samalas volcano has a maximum length of 7 km and a width of 5 km. Based on its volume (~15 ± 0.5 $km^3$), the average depth of the avalanche caldera would be ~430 m. The former scar of this caldera is not recognizable in the present topography. In the post-avalanche period, the scar was probably fully or partially covered by a new dome structure, which subsequently comprised the ~40 $km^3$ volcano edifice that collapsed during the 1257 CE eruption (Lavigne et al. 2013).

Although all VolcFlow simulations failed to enclose the original deposit, several factors may explain these discrepancies. The primary factor is attributed to the volume of removed material being larger than the calculated volume. The lack of stratigraphic data in the DAD region increases the uncertainty in calculating the volume (Bernard et al. 2021). The original volume of emplaced materials may exceed 20 $km^3$.

The second factor relates to the triggering mechanism. The occurrence of a directed blast may have influenced the widespread avalanche propagation. A Bandai-type eruption (Siebert et al. 1987), which is solely phreatic is unlikely to be the main cause of the debris avalanche at Samalas. We argue that the vast runout of Kalibabak DAD was possibly due to a Bezymianny-type eruption (a magmatic eruption) (Siebert et al. 1987) and likely accompanied by a lateral blast such as at Mount St. Helens in 1980 (Belousov et al. 2007; Siebert et al. 1987; Glicken 1996). However, it uncertain that a blast could have triggered the avalanche at Samalas volcano since no blast deposits have been found yet. Information on the Propok pumice and associated eruption that likely triggered the Kalibabak DAD also remain limited (Nasution et al. 2004; Métrich et al. 2017). Therefore, even if this eruption has been previously considered sub-Plinian, it is not impossible that it was of Plinian type.

The last factor is related to the paleo-topography of the south-eastern part of Lombok, which differs from the reconstructed DEM. The pre-collapse topography of this region may be more complex, with various valley forms. A channelised or valley-filling flow mechanism (Yoshida 2014) is proposed to involve the far-reaching deposition in the south-eastern part of the island. The morphological characteristics of DAD (Fig. 8a) and VolcFlow simulation results (Fig. 13) have supported this suggestion. The ancient valley of Kali Palung may have helped the DAD flow to be extended and channelised, resulting in a further runout towards this direction. An example of valley-filling DAD in Indonesia with a significant runout distance is the DAD from Raung volcano, which propagated through a broad valley between Iyang-Argapura Volcanic Complex and Meru Betiri Mountain (~10 km) (Moktikanana et al. 2021). Another example of channelised DAD is from Antocu volcano (Chile), which traveled through a relatively narrow (~6 km) river valley (Laja river) (Romero et al. 2022).

## Landform evolution

Volcanic activity has occurred in Lombok since the Pliocene (Zubaidah 2010). However, the stratigraphic framework in this region provides chronology since the Holocene (Nasution et al. 2004; Métrich et al. 2017). Volcanism was initiated by the stratocone building stage at 11 ka with predominantly effusive eruptions (Fig. 14), which then evolved into explosive eruptions. The climax occurred when a sub-Plinian (possibly Plinian) eruption likely led to a debris avalanche that mantled the southern flank and

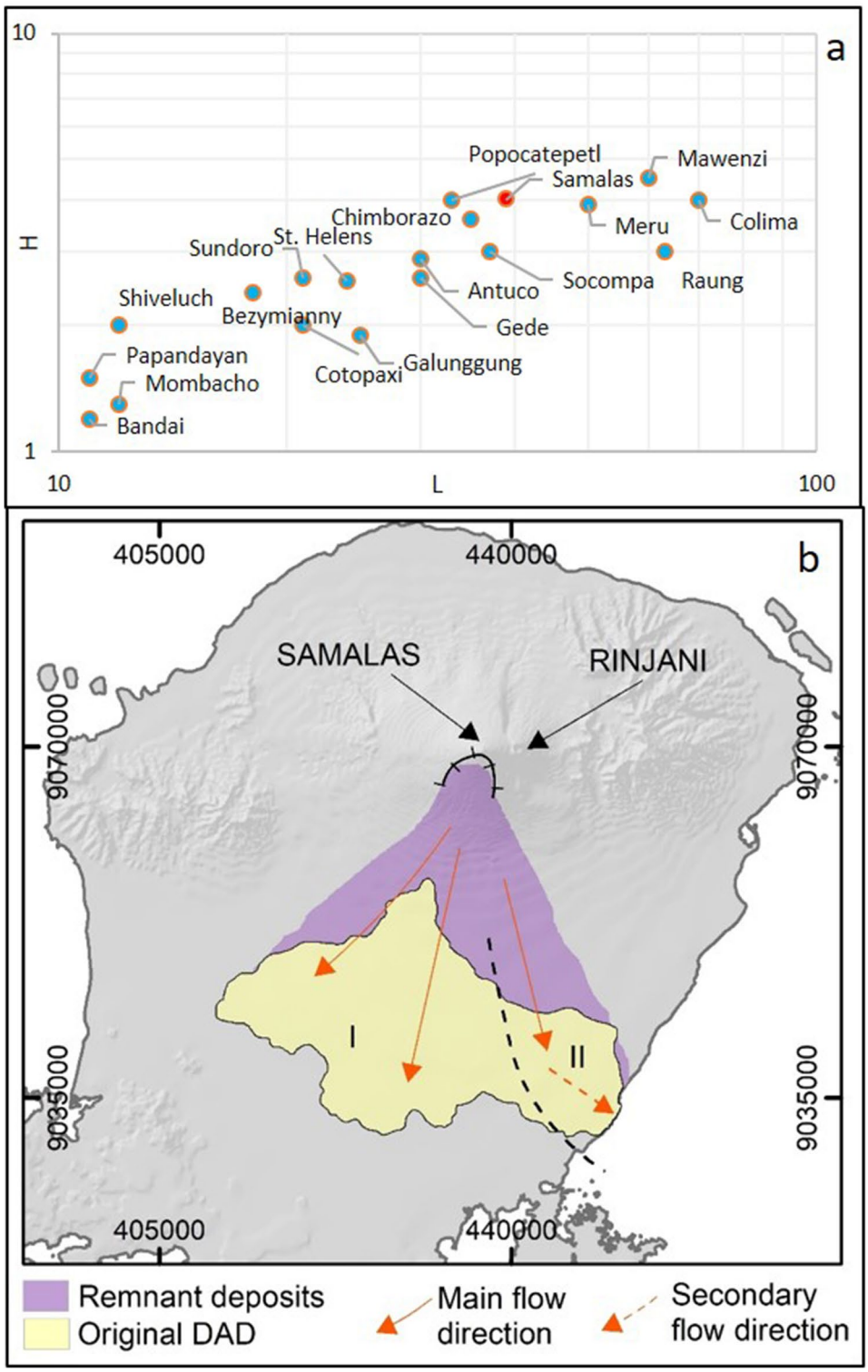


**Fig. 15** **a** Comparison of friction coefficient (H/L) for various debris avalanches worldwide (data from Siebert et al. 1987). **b** Emplacement dynamic of the Kalibabak debris avalanche from Samalas volcano

distal area of the volcano. The debris avalanche buried an area of 500-700 km$^2$ with a maximum runout distance of deposition of up to ~39 km. Although the modelling from VolcFlow produced an estimated velocity, the model failed to enclose the present deposit. Therefore, the runout velocity has been estimated using the friction loss and potential energy of avalanche run-up formula (Naranjo & Francis 1987) (Supplementary Material: Table S3). The calculation suggests the velocity of the debris avalanche was ~65 m/s, which results in a duration of about 10 minutes. With this high velocity, it is expected that significant erosion occurred during downstream travel. The triggering

mechanism and its velocity illustrate how large boulders can be dispersed over long distances.

After the complete deposition of the DAD, it is entered the post-avalanche stage, where erosion and resedimentation processes were initiated. Probably only a few lahars were generated during this stage due to the absence of abundant pyroclastic material. A fluvial modifying stage may have created new river channels (Manville et al. 2009), and slow mass-wasting likely occurred on the front lobes. The river channel stabilization continued to develop (Gran et al. 2011) and the volcano entered the new stratocone-building stage after the sector collapse.

A Plinian eruption attributed to Rinjani by Nasution et al. (2004) occurred between 800-500 BCE, which produced significant pumice dispersal (Rinjani pumice). Following this eruption, magma amalgamation occurred beneath the Samalas-Rinjani complex for ~2 kyr (Métrich et al. 2017). The large magma reservoir then sustained the Plinian eruption of 1257 CE through the Samalas vent resulting in the large caldera (~6 km) and voluminous PDC deposit (Lavigne et al. 2013). The PDCs mantled the wide area of Lombok in the SW, NW, N, NE, and SE directions (Vidal et al. 2015; Mutaqin et al. 2019). Similar to the DAD, PDCs aggraded the topography up to ~50 m. The dynamics of formation-destruction of the volcanic edifice in Samalas volcano may be similar to Usu volcano, Japan, which was destroyed by sector collapse and followed by Plinian eruption after a thousand-year gap (Goto et al. 2019). This sequence of volcanic activity demonstrates the dynamics of landscape following explosive eruptions, starting from landscape forming, mantling, and modifying (Manville et al. 2009). Lombok is an example of a region that significantly experienced abrupt landform evolution due to volcanic eruptions, particularly caused by sector collapse leading to a gigantic DAD and caldera-forming eruption leading to voluminous PDC. A similar explosive event that may cause voluminous PDCs or a gigantic DAD is possible associated with the stratocone adjacent to Samalas, namely Rinjani. Given that an active magma reservoir lies beneath Rinjani and Barujari vent, there is a risk of an explosive event (Metrich et al. 2017). However, for the moment, the activity of Rinjani is considered stable and the volcano has not any signal of destructive eruptions. The 2018 earthquake sequence also has no significant effect on the unrest of Rinjani volcano (Zhao et al. 2022).

## Conclusion

The present analysis of the Holocene Kalibabak debris avalanche of Samalas volcano shows that the observed DAD is one of the largest in the Asian region with a measured area of 535 $km^2$ and a volume of ~ 15 $km^3$. This fan-shaped DAD widened in the center (41 km) and had a runout distance up to 39 km from the source. The long runout distance of this DAD is attributed to the valley-filling distribution controlled by pre-avalanche topography, particularly in the south-eastern part of Lombok Island. The proposed age of this gigantic DAD is ~ 3,500 BCE. The Kalibabak DAD from Samalas volcano provides an example of the complexity in reconstructing past debris avalanche when the source-caldera has been completely erased (in the present case due to the 1257 CE caldera-forming eruption). It is challenging to determine the possible triggering factor of the debris avalanche because various juvenile and pyroclastic deposits above, below, or incorporated within the DAD were absent from the outcrops. A sub-Plinian eruption of the Samalas volcano may have been responsible for triggering the massive debris avalanche in Lombok Island.

**Supplementary Information** The online version contains supplementary material available at https://doi.org/10.1007/s00445-024-01727-7.

**Acknowledgements** Thanks to Kusnadi from the Department of Energy and Mineral Resources, West Nusa Tenggara Province, for providing coring data. Thanks to Hiden (RIP) from the Geophysics Department of Universitas Mataram (UNRAM), we are very grateful for your help during research in Lombok. We also thank Yayat Sudrajat and Lina Handayani from National Research and Innovation Agency of Indonesia (BRIN) who helped us in working with the resistivity data. Thanks to the Reviewers and Editors for their constructive comments. We would like to acknowledge the fieldwork team from UNRAM and Universitas Muhammadiyah Mataram, Hisyam, Fariq, Witari, Erna, and Arief for their help in collecting field data.

**Author Contributions** MNM and FL designed the research; PL and KK performed models; MNM and FL analyzed the data with the help from CG, PW and DSH; MNM, FL, DSH, S, and AF conducted field survey. All authors discussed the results and commented on the manuscript.

**Data Availability** All data are presented in manuscript. Any inquiries can be directed to the corresponding author.

## Declarations

**Conflict of interest** The authors declare that they have no conflict of interest.

## References

Abdul-Jabbar, G, Rachmat, H, Nakagawa, M (2019) Temporal change of Barujari Volcano magmatic process: Inferred from petrological study of erupted products since AD 1944. J Phys: Conf Ser, 1363(1). https://doi.org/10.1088/1742-6596/1363/1/012030

Andrade SD, van Wyk de Vries B (2010) Structural analysis of the early stages of catastrophic stratovolcano flank-collapse using analogue models. Bull Volcanol 72(7):771–789. https://doi.org/10.1007/s00445-010-0363-x

Belousov A, Belousova M, Voight B (1999) Multiple edifice failures, debris avalanches and associated eruptions in the Holocene history of Shiveluch volcano, Kamchatka. Russia Bulletin of Volcanology 61(5):324–342. https://doi.org/10.1007/s004450050300

Belousov A, Voight B, Belousova M (2007) Directed blasts and blast-generated pyroclastic density currents : a comparison of the Bezymianny 1956, Mount St Helens 1980, and Soufrière Hills, Montserrat 1997 eruptions and deposits. Bull Volcanol 69:701–740. https://doi.org/10.1007/s00445-006-0109-y

Bernard B, van Wyk de Vries B, Leyrit H (2009) Distinguishing volcanic debris avalanche deposits from their reworked products: the Perrier sequence (French Massif Central). Bull Volcanol 71(9):1041. https://doi.org/10.1007/s00445-009-0285-7

Bernard K, De Vries BVW, Thouret J (2019) Fault textures in volcanic debris-avalanche deposits and transformations into lahars: The Pichu Pichu thrust lobes in south Peru compared to worldwide avalanche deposits. J Volcanol Geotherm Res 371:116–136

Bernard B, Takarada S, Andrade SD, Dufresne A (2021) Terminology and strategy to describe large volcanic landslides and debris avalanches. In: Roverato M, Dufresne A, Procter J (eds) Volcanic debris avalanches. Advances in volcanology. Springer, Cham. https://doi.org/10.1007/978-3-030-57411-6_3

Bronto S, Ratdomopurbo A, Asmoro P, Adityarani M (2014) Longsoran Raksasa Gunung Api Merapi Yogyakarta – Jawa Tengah (Giant landslide in Merapi volcano Yogyakarta-Central Java). Jurnal Geologi Dan Sumberdaya Mineral 15(5):165–183. https://doi.org/10.33332/jgsm.geologi.v15i4

Bronto S (1989) Volcanic geology of Galunggung, West Java, Indonesia. 511. http://ir.canterbury.ac.nz/handle/10092/5667. Accessed 06 Jan 2023

Calvari S, Tanner LH, Groppelli G, Norini G (2004) Valle del Bove, eastern flank of Etna volcano: a comprehensive model for the opening of the depression and implications for future hazards. American Geophysical Union, In Etna Volcano Laboratory

Camus, G, Diament, M, Gloaguen, M (1992) Emplacement of a Debris Avalanche during the 1883 Eruption of Krakatau Emplacement of a Debris Avalanche during the 1883 Eruption of Krakatau (Sunda Straits, Indonesia). Geo J, September. https://doi.org/10.1007/BF00177224

Capra L, Macías JL, Scott KM, Abrams M, Garduño-Monroy VH (2002) Debris avalanches and debris flows transformed from collapses in the Trans-Mexican Volcanic Belt, Mexico – behavior, and implications for hazard assessment. J Volcanol Geoth Res 113(1):81–110. https://doi.org/10.1016/S0377-0273(01)00252-9

Cortés A, Macías JL, Capra L, Garduño-monroy VH (2010) Sector collapse of the SW fl ank of Volcán de Colima, México The 3600 yr BP La Lumbre – Los Ganchos debris avalanche and associated debris fl ows. J Volcanol Geoth Res 197:52–66. https://doi.org/10.1016/j.jvolgeores.2009.11.013

Davies TR, McSaveney MJ, Hodgson KA (1999) A fragmentation-spreading model for long-runout rock avalanches. Can Geotech J 36(6):1096–1110. https://doi.org/10.1139/t99-067

Dibacto S, Lahitte P, Karátson D, Hencz M, Szakács A, Biró T, Kovács I, Veres D (2020) Growth and erosion rates of the East Carpathians volcanoes constrained by numerical models: Tectonic and climatic implications. Geomorphology 368:107352. https://doi.org/10.1016/j.geomorph.2020.107352

Dufresne A, Davies TR (2009) Longitudinal ridges in mass movement deposits. Geomorphology 105(3–4):171–181. https://doi.org/10.1016/j.geomorph.2008.09.009

Dufresne, A, Siebert, L, Bernard, B (2021) Distribution and Geometric Parameters of Volcanic Debris Avalanche Deposits BT - Volcanic Debris Avalanches: From Collapse to Hazard (M. Roverato, A. Dufresne, & J. Procter, Eds.; pp. 75–90). Springer International Publishing. https://doi.org/10.1007/978-3-030-57411-6_4

Ferrario MF (2019) Landslides triggered by multiple earthquakes: insights from the 2018 Lombok (Indonesia) events. Nat Hazards 98(2):575–592. https://doi.org/10.1007/s11069-019-03718-w

Garajeh MK, Feizizadeh B, Blaschke T, Lakes T (2022) Detecting and mapping karst landforms using object-based image analysis: Case study: Takht-Soleiman and Parava Mountains. Iran Egypt J Remote Sens Space Sci 25(2):473–489. https://doi.org/10.1016/j.ejrs.2022.03.009

Glicken H (1996) Rockslide-debris Avalanche of May 18, 1980, Mount St. Helens Volcano, Washington: U.S. Geological Survey Open-File Report 96–677, p 90, 5 plates. https://pubs.usgs.gov/of/1996/0677/

Goto, Y, Danhara, T, Tomiya, A (2019) Catastrophic sector collapse at Usu volcano, Hokkaido, Japan: failure of a young edifice built on soft substratum. Bull Volcanol, 81(6). https://doi.org/10.1007/s00445-019-1293-x

Gran KB, Montgomery DR, Halbur JC (2011) Long-term elevated post-eruption sedimentation at Mount Pinatubo. Philippines Geol 39(4):367–370. https://doi.org/10.1130/G31682.1

Grilli ST, Tappin DR, Carey S, Watt SFL, Ward SN, Grilli AR, Engwell SL, Zhang C, Kirby JT, Schambach L, Muin M (2019) Modelling of the tsunami from the December 22, 2018 lateral collapse of Anak Krakatau volcano in the Sunda Straits. Indonesia Sci Rep 9(1):11946. https://doi.org/10.1038/s41598-019-48327-6

Grosse P, Danišík M, Apaza FD, Guzmán SR, Lahitte P, Quidelleur X, Self S, Siebe C, van Wyk de Vries B, Ureta G, Guillong M, De Rosa R, Le Roux P, Wotzlaw JF, Bachmann O (2022) Holocene collapse of Socompa volcano and pre- and post-collapse growth rates constrained by multi-system geochronology. Bull Volcanol 84(9):1–18. https://doi.org/10.1007/s00445-022-01594-0

Harsuko, MRC, Zulfakriza, Z, Nugraha, AD, Sarjan, AFN, Widiyantoro, S, Rosalia, S, Puspito, NT, Sahara, DP (2020) Investigation of Hilbert – Huang Transform and Fourier Transform for Horizontal-to-Vertical Spectral Ratio Analysis : Understanding the Shallow Structure in Mataram City , Lombok , Indonesia. Front Earth Sci, 8(334). https://doi.org/10.3389/feart.2020.00334

Hayakawa YS, Yoshida H, Obanawa H, Naruhashi R, Okumura K, Zaiki M, Kontani R (2018) Characteristics of debris avalanche deposits inferred from source volume estimate and hummock morphology around Mt. Erciyes, central Turkey. Natur Hazards Earth Syst Sci 18(2):429–444. https://doi.org/10.5194/nhess-18-429-2018

Hogg AG, Heaton TJ, Hua Q, Palmer JG, Turney CSM, Southon J, Bayliss A, Blackwell PG, Boswijk G, Bronk Ramsey C, Pearson C, Petchey F, Reimer P, Reimer R, Wacker L (2020) SHCal20 Southern Hemisphere Calibration, 0–55,000 Years cal BP. Radiocarbon 62(4):759–778. https://doi.org/10.1017/RDC.2020.59

Hunt JE, Cassidy M, Talling PJ (2018) Multi-stage volcanic island flank collapses with coeval explosive caldera-forming eruptions. Sci Rep 8(1):1–11. https://doi.org/10.1038/s41598-018-19285-2

Kelfoun K, Druitt TH (2005) Numerical modeling of the emplacement of Socompa rock avalanche, Chile. J Geophys Res: Solid Earth 110(12):1–13. https://doi.org/10.1029/2005JB003758

Kelfoun, K, Giachetti, T, Labazuy, P (2010) Landslide-generated tsunamis at Réunion Island. J Geophys Res: Earth Surface, 115(F4). https://doi.org/10.1029/2009JF001381

Kelfoun, K (2011) Suitability of simple rheological laws for the numerical simulation of dense pyroclastic flows and long-runout volcanic avalanches. J Geophys Res: Solid Earth, 116(8). https://doi.org/10.1029/2010JB007622

Lahitte P, Samper A, Quidelleur X (2012) DEM-based reconstruction of southern Basse-Terre volcanoes (Guadeloupe archipelago, FWI): Contribution to the Lesser Antilles Arc construction rates and magma production. Geomorphology 136(1):148–164. https://doi.org/10.1016/j.geomorph.2011.04.008

Lavigne F, Degeai JP, Komorowski JC, Guillet S, Robert V, Lahitte P, Oppenheimer C, Stoffel M, Vidal CM, Pratomo Suronoh I, Wassmer P, Hajdas I, Hadmoko DS, De Belizal E (2013) Source of the great AD 1257 mystery eruption unveiled, Samalas volcano, Rinjani Volcanic Complex, Indonesia. Proc Natl Acad Sci USA 110(42):16742–16747. https://doi.org/10.1073/pnas.1307520110

Lomoschitz A, Hervás J, Yepes J, Meco J (2008) Characterisation of a pleistocene debris-avalanche deposit in the Tenteniguada Basin, Gran Canaria Island. Spain Landslides 5(2):227–234. https://doi.org/10.1007/s10346-008-0115-6

MacLeod N (1989) Sector-failure eruptions in Indonesian volcanoes. Geol Indonesia 12:563–601

Malawani, MN, Lavigne, F, Hadmoko, DS, Marfai, MA, Mutaqin, BW (2020) Hummocky terrain of the Kalibabak debris avalanche deposit, Lombok Island , Indonesia. E3S Web of Conferences, 200(02015). https://doi.org/10.1051/e3sconf/202020002015

Malawani, MN, Lavigne, F, Hadmoko, DS, Syamsuddin, S, Handayani, L, Sudrajat, Y, Virmoux, C, Saulnier Copard, S, Kusnadi, K (2023) Coastal sedimentation and topographic changes in the Mataram Plain, Lombok (Indonesia) following the 1257 CE eruption of Samalas volcano. Earth Surface Processes and Landforms, n/a(n/a). https://doi.org/10.1002/esp.5592

Mangga S, Atmawinata S, Hermanto B, Setyogroho B, Amin T (1994) Geological map of the Lombok Sheet, West Nusatenggara. Geological Research and Development Centre. https://geologi.esdm.go.id/geomap/pages/preview/peta-geologi-lembar-lombok-nusatenggara-barat

Manville V, Segschneider B, Newton E, White JDL, Houghton BF, Wilson CJN (2009) Environmental impact of the 1. 8 ka Taupo eruption, New Zealand : Landscape responses to a large-scale explosive rhyolite eruption. Sedimentary Geology 220(3–4):318–336. https://doi.org/10.1016/j.sedgeo.2009.04.017

Maryanto S (2009) Distribusi ukuran butir matriks breksi gunungapi di daerah Lombok Timur, Nusa Tenggara Barat. Bull Sci Contribution 7(1):49–71. https://doi.org/10.24198/bsc%20geology.v7i1.8233

Maryanto S, Hasan R, Siregar DA (2009) Mineralogi matriks breksi gunung api plistosen akhir – kuarter berdasarkan data XRD di daerah lombok timur, nusa tenggara barat. Jurnal Geologi Dan Sumberdaya Mineral 19(1). https://doi.org/10.33332/jgsm.geologi.v19i1.189

Métrich N, Vidal CM, Komorowski JC, Pratomo I, Michel A, Kartadinata N, Prambada O, Rachmat H, Surono (2017) New insights into magma differentiation and storage in holocene crustal reservoirs of the lesser sunda arc: The Rinjani-Samalas volcanic complex (Lombok, Indonesia). J Petrol 58(11):2257–2284. https://doi.org/10.1093/petrology/egy006

Moktikanana MLA, Wibowo HE, Rahayu E, Harijoko A (2021) Hummock size and alignment in Gadung debris avalanche deposit, Raung Volcanic Complex, East Java, Indonesia. IOP Conf Ser: Earth Environ Sci 851(1):012037. https://doi.org/10.1088/1755-1315/851/1/012037

Mutaqin BW, Lavigne F, Sudrajat Y, Handayani L, Lahitte P, Virmoux C, Hiden H, Komorowski DS, Hananto JC, Wassmer ND, Hartono P, Boillot-Airaksinen K (2019) Landscape evolution on the eastern part of Lombok (Indonesia) related to the 1257 CE eruption of the Samalas Volcano. Geomorphology 327:338–350. https://doi.org/10.1016/j.geomorph.2018.11.010

Naranjo JA, Francis P (1987) High velocity debris avalanche at Lastarria volcano in the north Chilean Andes. Bull Volcanol 49(2):509–514. https://doi.org/10.1007/BF01245476

Nasution A, Takada A, Mulyana R (2004) The volcanic activity of Rinjani, Lombok Island, Indonesia during the las ten thousand years, viewd from 14C age datings Proceeding of the 33rd Annual Convention and Exhibition. Indonesian Association of Geologist, Bandung

Norini, G, Bustos, E, Arnosio, M, Baez, W, Zuluaga, MC, Roverato, M (2020) Unusual volcanic instability and sector collapse configuration at Chimpa volcano, central Andes. J Volcanol Geothermal Res, 393. https://doi.org/10.1016/j.jvolgeores.2020.106807

Özdemir Y, Akkaya İ, Oyan V, Kelfoun K (2016) A debris avalanche at Süphan stratovolcano (Turkey) and implications for hazard evaluation. Bull Volcanol 78(2):1–13. https://doi.org/10.1007/s00445-016-1007-6

Paguican EMR, van Wyk de Vries B, Lagmay AMF (2014) Hummocks: how they form and how they evolve in rockslide-debris avalanches. Landslides 11(1):67–80. https://doi.org/10.1007/s10346-012-0368-y

Paris R, Bravo JJC, González MEM, Kelfoun K, Nauret F (2017) Explosive eruption, flank collapse and megatsunami at Tenerife ca. 170 ka. Nature Commun 8(2016):1–8. https://doi.org/10.1038/ncomms15246

Ponomareva VV, Pevzner MM, Melekestsev IV (1998) Large debris avalanches and associated eruptions in the Holocene eruptive history of Shiveluch volcano, Kamchatka. Russia Bull Volcanol 59(7):490–505. https://doi.org/10.1007/s004450050206

Pratomo I (2006) Klasifikasi Gunung Api Aktif Indonesia, Studi Kasus Dari Beberapa Letusan Gunung Api Dalam Sejarah (Classification of Indonesian active volcano" case study from several historic eruptions). Indonesian J Geosci 1(4):209–227. https://doi.org/10.17014/ijog.1.4.209-227

Procter, JN, Zernack, AV, Cronin, SJ (2021) Computer Simulation of a Volcanic Debris Avalanche from Mt. Taranaki, New Zealand BT - Volcanic Debris Avalanches: From Collapse to Hazard (M. Roverato, A. Dufresne, & J. Procter, Eds.; pp. 281–310). Springer International Publishing. https://doi.org/10.1007/978-3-030-57411-6_11

Rachmat H, Rosana M, Wirakusumah AD, Jabbar GA (2016) Petrogenesis of Rinjani post-1257 caldera-forming -eruption lava flows. Indonesian J Geosci 3(2):107–126. https://doi.org/10.17014/ijog.3.2.107-126

Romero JE, Moreno H, Polacci M, Burton M, Guzmán D (2022) Mid-Holocene lateral collapse of Antuco volcano (Chile): debris avalanche deposit features, emplacement dynamics, and impacts. Landslides 19(6):1321–1338. https://doi.org/10.1007/s10346-022-01865-z

Roverato M, Capra L, Sulpizio R, Norini G (2011) Stratigraphic reconstruction of two debris avalanche deposits at Colima Volcano (Mexico): Insights into pre-failure conditions and climate influence. J Volcanol Geoth Res 207(1–2):33–46. https://doi.org/10.1016/j.jvolgeores.2011.07.003

Salinas S, López-Blanco J (2010) Geomorphic assessment of the debris avalanche deposit from the Jocotitlán volcano. Central Mexico Geomorphology 123(1–2):142–153. https://doi.org/10.1016/j.geomorph.2010.07.006

Shea T, van Wyk de Vries B, Pilato M (2008) Emplacement mechanisms of contrasting debris avalanches at Volcán Mombacho (Nicaragua), provided by structural and facies analysis. Bull Volcanol 70(8):899–921. https://doi.org/10.1007/s00445-007-0177-7

Siebert L (1984) Large volcanic debris avalanches: Characteristics of source areas, deposits, and associated eruptions. J Volcanol Geoth Res 22(3–4):163–197. https://doi.org/10.1016/0377-0273(84)90002-7

Siebert L (2002) Landslide resulting from structural failureof volcanoes. In: Evans SG, De Graff JV (eds) Catastrophic landslide: effects, occurrence, and mechanisms. Geological Society of America Reviews in Engineering Geology, pp 209–235

Siebert L, Glicken H, Ui T (1987) Volcanic hazards from Bezymianny- and Bandai-type eruptions. Bull Volcanol 49(1):435–459. https://doi.org/10.1007/BF01046635

Siebert L, Beget JE, Glicken H (1995) The 1883 and late-prehistoric eruptions of Augustine volcano, Alaska. J Volcanol Geoth Res 66:367–395

Siebert, L, Roverato, M (2021) A Historical Perspective on Lateral Collapse and Volcanic Debris Avalanches. In M. Roverato, A. Dufresne, & J. Procter (Eds.), Volcanic Debris Avalanches: From Collapse to Hazard (pp. 11–50). Springer International Publishing. https://doi.org/10.1007/978-3-030-57411-6_2

Solikhin A, Kunrat S, Barbier B, Campion R (2010) Geochemical and Thermodinamic Modeling of Segara Anak Lake and the 2009 Eruption of Rinjani Volcano, Lombok. Indonesia Jurnal Geologi Indonesia 5(4):227–239

Stuiver M, Reimer PJ (1993) Extended 14C data base and revised CALIB 3.0 14C age calibration program. Radiocarbon 35(1):215–230

Sukandi (2017) Resistivity measurement for mapping groundwater potential at praya regional general hospital (in bahasa). Sangkareang 3(3):66–71

Tibaldi A (2001) Multiple sector collapses at Stromboli volcano, Italy: How they work. Bull Volcanol 63(2–3):112–125. https://doi.org/10.1007/s004450100129

Ui T, Yamamoto H, Suzuki-Kamata K (1986) Characterization of debris avalanche deposits in Japan. J Volcanol Geoth Res 29:231–243

Ui, T (1989) Discrimination Between Debris Avalanches and Other Volcaniclastic Deposits. In J. H. Letter (Ed.), AVCEI Proceedings in Volcanology. Springer-Verlag Berlin Heidelberg. https://doi.org/10.1007/978-3-642-73759-6_13

Valverde V, Mothes PA, Beate B, Bernard J (2021) Enormous and far-reaching debris avalanche deposits from Sangay volcano (Ecuador): Multidisciplinary study and modeling the 30 ka sector collapse. 411. https://doi.org/10.1016/j.jvolgeores.2021.107172

van Wyk de Vries, B, Davies, T (2015) Chapter 38 - Landslides, Debris Avalanches, and Volcanic Gravitational Deformation. In H. Sigurdsson (Ed.), The Encyclopedia of Volcanoes (Second Edition) (pp. 665–685). Academic Press. https://doi.org/10.1016/B978-0-12-385938-9.00038-9

Vezzoli L, Apuani T, Corazzato C, Uttini A (2017) Geological and geotechnical characterization of the debris avalanche and pyroclastic deposits of Cotopaxi Volcano (Ecuador). A contribute to instability-related hazard studies. J Volcanol Geoth Res 332:51–70. https://doi.org/10.1016/j.jvolgeores.2017.01.004

Vidal, CM, Komorowski, JC, Métrich, N, Pratomo, I, Kartadinata, N, Prambada, O, Michel, A, Carazzo, G, Lavigne, F, Rodysill, J, Fontijn, K, Surono (2015) Dynamics of the major Plinian eruption of Samalas in 1257 A.D. (Lombok, Indonesia). Bulletin of Volcanology, 77(9). https://doi.org/10.1007/s00445-015-0960-9

Voight B, Janda RJ, Glicken H (1983) Nature and mechanics of the mount St Helens rockslide avalanche of 18 May 1980. Geotechnique 33(3):243–273. https://doi.org/10.1016/0148-9062(83)90666-6

Voight B, Janda RJH, Glicken, Douglas PM (1985) Nature and mechanics of the Mount St Helens rockslide-avalanche of 18 May 1980. Geotechnique 35(3):357–368. https://doi.org/10.1680/geot.1985.35.3.357

Wibowo, SB, Hadmoko, DS, Isnaeni, Y, Farda, NM, Febri, A, Putri, S, Nurani, IW, Supangkat, SH (2021) Spatio-Temporal Distribution of Ground Deformation Due to 2018 Lombok Earthquake Series. Remote Sens, 13(2222). https://doi.org/10.3390/rs13112222

Wiranata A, Soekarno S, Suroso A (2018) Estimation of groundwater potential with geoelectric method in Central Lombok Regency (in Bahasa). In Artikel Ilmiah (Unpublished thesis). Civil Engineering, Universitas Mataram. http://eprints.unram.ac.id/id/eprint/5785

Yoshida H (2013) Decrease of size of hummocks with downstream distance in the rockslide-debris avalanche deposit at Iriga volcano, Philippines: Similarities with Japanese avalanches. Landslides 10(5):665–672. https://doi.org/10.1007/s10346-013-0414-4

Yoshida H (2014) Hummock alignment in Japanese volcanic debris avalanches controlled by pre-avalanche slope of depositional area. Geomorphology 223:67–80. https://doi.org/10.1016/j.geomorph.2014.06.024

Zhao, S, McClusky, S, Miller, M, Cummins, P, Garthwaite, M (2022) The influence of the 2018 Lombok earthquake sequence, Indonesia on the unrest Rinjani volcano inferred from InSAR time-series analysis, EGU General Assembly 2022, Vienna, Austria, 23–27 May 2022, EGU22-3579. https://doi.org/10.5194/egusphere-egu22-3579

Zubaidah, T (2010) Spatio-temporal characteristics of the geomagnetic field over the Lombok Island, the Lesser Sunda Islands region: New geological, tectonic, and seismo-electromagnetic insights along the Sunda-Banda Arcs transition [PhD Thesis, (Scientific Technical Report), Deutsche GeoForschungsZentrum GFZ]. https://doi.org/10.2312/GFZ.b103-10079